DEVELOPMENT OF MP-SPR BIOSENSOR ANALYSIS METHOLOGY

Juha Mäkinen
Master´s thesis
Faculty of Medicine and Life Sciences
University of Tampere
August 25, 2017

PRO GRADU –TUTKIELMA

Paikka: TAMPEREEN YLIOPISTO
Lääketieteen ja biotieteiden tiedekunta
Tekijä: MÄKINEN, JUHA PEKKA
Otsikko: MP-SPR biosensorimittausten analyysimenetelmien kehittäminen
Sivut: 76
Ohjaajat: FT Jenni Leppiniemi, FT Inger Vikholm-Lundin, FT Niko Granqvist, FM Jussi Tuppurainen ja apulaisprofessori Vesa Hytönen
Tarkastajat: Apulaisprofessori Vesa Hytönen ja FT Martin Albers
Aika: 25.08.2017

Tiivistelmä

Optiset biosensorit ovat saaneet arvostusta lukuisissa käyttökohteissa, kuten lääketeollisuudessa ja kliinisessä diagnostiikassa, biologisen tunnistuselementin korkean spesifisyyden ja optisen detektiomenetelmän non-invasiivisuuden ansiosta. Optisen biosensorien tehokas ja joustava käyttö kuitenkin edellyttää, että käyttäjä ymmärtää näiden toiminnan fysikaalisia, kemiallisia ja biologisia perusperiaatteita sekä optisten menetelmien etuja ja rajoituksia. Tutkielman kirjallinen osa tutustuttaa biosensoreiden ja biosensoroinnin perusteisiin sekä esittelee erään optiseen pintaplasmoniresonanssiin (surface plasmon resonance, SPR) perustuvan laitteiston toimintaa, etuja ja haasteita.

Tutkielman kokeellisissa osuuksissa käytettiin multiparametrista SPR-laitteistoa (MP-SPR), joka kykenee mittaamaan molekyylien adsorption lisäksi laajasti näytteen optisia ominaisuuksia. Proteiiniliuoksien konsentraatiot sekä niiden puhtausasteet määritettiin UV-Vis-spektrofotometrilla.

Tutkielman ensimmäinen kokeellinen osuus osoitti switchavidiiniin (neutralisoitu avidiinimutantti) ja proteiini G molekyyleihin perustuvan regeneroitavan immunosensorointipinnan toistettavuuden ja vertailtavuuden. Lisäksi sensorointipinta osoitti, että proteiinien non-spesifinen sitoutuminen on erittäin vähäistä eräillä malliproteiineilla tutkittaessa. IgG-molekyylien immobisaation toimivuudesta ei kuitenkaan saatu luotettavia tuloksia. Lisäksi tutkielma esittää switchavidiinille MP-SPR mittausdataan perustuvan mekaanisen sitoutumismallin. Jatkotutkimuksissa voitaisiin keskittyä monimutkaisempien näytteiden mittaamiseen sekä kehittää esitettyyn sitoutumismalliin perustuvaa automaatiota.

Tutkielman toinen kokeellinen osuus tutki nelikanavaisen MP-SPR-prototyypin soveltuvuutta nopeasti sitoutuvien pienlääkemolekyylien sitoutumisen mittaamiseen. Ihmisen hiilihappoanhydraasi II-entsyymiä immobilisoitiin kolmiulotteiseen hydrogeelimatriksiin ja kolmen sulfonamidi-inhibiittorin sitoutumiskinetiikkaa vertailtiin referenssiartikkelin tuloksiin. Tutkimuksessa onnistuttiin mittaamaan ja analysoimaan kineettiset vakiot vain yhdestä inhibiittorista (asetatsoliamidi). Johtopäätöksenä MP-SPR-prototyyppi kykenee mittaamaan pienmolekyylien nopeaa sitoutumiskinetiikkaa, mutta tämän edellytyksenä on erittäin tarkka näytteiden ja puskureiden valmistus sekä bulkkivasteiden oikeaoppinen kalibraatio.

Avainsanat: pintaplasmoniresonanssi, kliininen diagnostiikka, farmakodynamiikka, assay-kehitys, sitoutumiskinetiikka, avidiini-biotiini-teknologia pienlääkemolekyylit, proteiinien adsorptiomallit

MASTER´S THESIS

Place: UNIVERSITY OF TAMPERE
Faculty of Medicine and Life Sciences
Author: MÄKINEN, JUHA PEKKA
Title: Development of MP-SPR biosensor analysis methology
Pages: 76
Supervisors: Ph.D. Jenni Leppiniemi, Ph.D. Inger Vikholm-Lundin, Ph.D. Niko Granqvist, M.Sc. Jussi Tuppurainen and associate professor Vesa Hytönen
Reviewers: Associate professor Vesa Hytönen and Ph.D. Martin Albers
Date: August 25, 2017

Abstract

Optical biosensors have gained high regard in the field of drug industry and clinical diagnostics owing to the high specificity of biological recognition elements as well as to the non-invasiveness of optical detection methods. The flexible and efficient use of optical biosensors, however, requires that the user understands their basic physical, chemical, and biological principles as well as the advantages and limitations of these devices. The literature review introduces the fundamentals of biosensing and biosensors, and describes the principles, advantages and challenges related to one type of surface plasmon resonance (SPR) device.

In the experimental part of the thesis, a multiparametric SPR (MP-SPR)-system was used to measure the optical properties of samples in addition to the traditional adsorption of molecules. The concentrations and purity of protein solutions were determined by a UV-Vis spectrophotometer.

The first experimental part showed the reproducibility and repeatability of a regenerable IgG-sensing surface prepared using switchavidin (a neutralized avidin mutant) and protein G molecules. Furthermore, the sensing surface has ultralow fouling ability against some common model proteins. The immobilization of IgG-molecules did not show, however, reliable results. Additionally, the thesis represents a mechanical model for the switchavidin adsorption that is based on the MP-SPR measurement data. Further research could concentrate on the measurement of more complex samples as well as on the development of automation that is based on the represented mechanical adsorption model.

The second experimental part studied the applicability of a four-channel MP-SPR prototype into the measurement of fast association kinetics of small molecular weight (MW) drugs. A human carbonic anhydrase II enzyme was immobilized into a three-dimensional hydrogel matrix and the interaction kinetics of three sulfonamide inhibitors were compared with kinetic values in the literature. Only a single inhibitor (acetazolamide) gave satisfying results. In conclusion, the MP-SPR-prototype is capable of measuring the fast association kinetics of small MW drugs, but this requires the very accurate preparation of samples and buffers as well as the proper calibration of bulk responses.

Keywords: surface plasmon resonance, clinical diagnostics, pharmacodynamics, assay development, interaction kinetics, avidin technology, small drug molecules, adsorption models of proteins

ACKNOWLEDGEMENTS

The experimental part of Master's thesis was conducted in the Protein Dynamics research group of the Faculty of Medicine and Life Sciences (the University of Tampere) and involved notable contribution from the company BioNavis. The research group applies experimental and computational methods to study structure-function relationships as well as to develop new vaccines, biofunctionalized materials, and diagnostic tools. The BioNavis develops and markets multiparametric surface plasmon resonance (MP-SPR) spectroscopy instruments.

The research group leader Dr. Vesa Hytönen together with Inger Vikholm-Lundin, Ph.D., and Jenni Leppiniemi, Ph.D. were responsible for the academic supervision and valuable advice concerning laboratory practice. The research group provided also access to protein bank samples. Jussi Tuppurainen, M.Sc. and Niko Granqvist, Ph.D. from the BioNavis company provided expertise and support concerning the surface plasmon resonance technology and instrumentation. The company also covered new reagents and materials that were not available from other sources, e.g. the other research groups of the Faculty of Medicine and Life Sciences. I would like to acknowledge the professional support of my supervisors. They gave me valuable advice how to improve academic output, and taught me how to profit from the versatile features of the surface plasmon resonance technology.

Huge thanks go to people who donated me proteins and shared their know-how about varying subjects. Martin Albers from the BioNavis company kindly produced all the biotinylated gold sensors used in the first part of the Master's thesis, repaired the MP-SPR instruments when needed, and delivered consumables and accessories during the experimental work. Niklas Kähkönen from the Protein Dynamics research group produced and purified switchavidin used in the sensing platform construction. Inger Vikholm-Lundin from the Protein Dynamics research group, and Jorma Isola, M.D., Ph.D. from the Cancer Biology research group of the Faculty of Medicine and Life Sciences contributed to the experimental work by providing the antibodies used in the Master's thesis. Seppo Parkkila, M.D., Ph.D. and Marianne Kuuslahti from the Tissue Biology research group (Faculty of Medicine and Life Sciences, the University of Tampere) kindly provided human carbonic anhydrase II enzyme for the experiments conducted in the second part of the thesis. Anna-Maija Koivisto, M.Sc. from the School of Health Sciences helped me to resolve some of the challenges related to the statistical analysis and data interpretation of the datasets. Tony Stoor from BioNavis gave me valuable information about the instrumentation issues of MP-SPR Navi™ devices.

Finally, I also want to express my deep gratitude and appreciation for my family. You encouraged and supported me in the good and the bad days during the whole project.

Contents

ABBREVIATIONS

α-CA	α-class carbonic anhydrase enzyme
AZE	Acetazolamide
BAT	Biotin-terminated alkanethiol
b-SAM	Biotinylated self-assembled monolayer
b-SLB	Biotinylated supported lipid bilayer
4-CBS	4-sulfamoylbenzoic acid
CMD	Carboxymethyl-dextran
CV	Coefficient of variation
DLS	Dynamic light scattering
DMSO	Dimethyl sulfoxide
EDC	N-(3-dimethylaminopropyl)-N′-ethylcarbodiimide hydrochloride
ELISA	Enzyme-linked immunosorbent assay
FC	Flow channel
hCAII	Human carbonic anhydrase II enzyme
h-IgG	Immunoglobulin gamma from human blood serum
LOD	Limit of detection
LSPR	Localized surface plasmon resonance
MAT	Matrix alkanethiol
mDeg	Millidegree unit of angle
MES	2-(N-morpholino)ethanesulfonic acid
MP-SPR	Multiparametric surface plasmon resonance
MSU	Methanesulfonamide
MTL	Mass transport limitation
MW	Molecular weight
MWCO	Molecular weight cutoff
NCAvd	Neutralized chimeric avidin
NHS	N-hydroxysuccinimide
NP	Nanoparticle
PDMS	Poly(dimethylsiloxane)
PEEK	Poly(ether ether ketone)
PMI	SPR peak minimum intensity
QCM-D	Quartz crystal microbalance with dissipation
RI	Refractive index
RT	Room temperature
RU	Response unit
SD	Sample standard deviation
SDS	Sodium dodecyl sulfate
SE	Spectroscopic ellipsometry
SPR	Surface plasmon resonance
TIR	Total internal reflection
UV-Vis	Ultraviolet – visible light (spectrum)

1 INTRODUCTION

The drug research and clinical diagnostics have exploited the natural binding mechanisms of biomolecules for several decades (Clark 1956). In biosensing technology, the use of biological recognition elements (i.e. ligand) usually results in the high affinity and specificity of analyte binding. This also enables the determination of biological activity with interaction kinetics that is practically impossible with chemical sensors. When the generated signal is transduced from an optical format into an electrical current, the detection system does not affect the properties of the sample. The flexible and effective use of optical biosensors, however, requires biological, chemical, and physical knowledge about the design and function of the optical biosensing surfaces and instrumentation. The main purpose of this thesis is to give a theoretical background about the principles of optical biosensing and the construction of a functional bioassay. Furthermore, it depicts the practical benefits and disadvantages of optical real-time biosensing using a unique multiparametric surface plasmon resonance (MP-SPR) instrumentation from BioNavis Ltd. The MP-SPR system simultaneously follows the scattering and absorbance properties of the adsorption layer as well as the bulk changes in addition to the traditional SPR peak minimum angle (Viitala *et al.* 2013).

Trustful and repeatable measurement of biomarkers from complex media such as blood serum requires an accurate, precise, and reproducible sensing system with anti-fouling and regeneration properties. To reach these goals, an optical immunosensor, which utilizes biotinylated protein G and switchavidin molecules to orient IgG molecules and to achieve separate regeneration steps for the IgG layer and the layers above it, had been designed by numerous research groups (Pollheimer *et al.* 2013). The experiments conducted in the first experimental part of this thesis adapted the protocol described in the article of Zauner *et al.* 2016 to reconstruct, assess, and optimize the immunosensing platform using the MP-SPR detection system.

The α-class carbonic anhydrases (α-CAs) that are found from mammals have significant roles in numerous physiological and pathological processes, such as pH and CO_2 homeostasis, biosynthetic reactions, tumorigenicity, and electrolyte secretion in multiple tissues/organs (Rogez-Florent *et al.* 2014). Logistically, humans have several isoforms of α-CAs with separate functions in distinct locations in many tissues/organs. This underlines the importance of directed research that is focused on designing highly target-selective inhibitors to minimize the

side effects of drugs. The traditional way to collect only thermodynamic data, such as a dissociation constant (K_D), leads to a loss of valuable information that would otherwise enhance the process of drug discovery, or explain the rapid course of a disease as well as the resistance to drug therapy. The unavoidable challenge, however, arises from the fast association kinetics of sulfonamide inhibitors combined with the small molecular weight (MW). In the second experimental part of this thesis, the interaction kinetics of the human carbonic anhydrase (hCAII) enzyme with the sulfonamide inhibitors was studied in order to test the kinetic limits of a four-channel MP-SPR prototype, and to verify the fast association kinetics of sulfonamide inhibitors using the angular scan mode of MP-SPR instrumentation. The experiments followed the protocol described in an article of Papalia and colleagues in 2006 with minor modifications.

2 LITERATURE REVIEW

2.1 Fundamentals of optical biosensing

Optical biosensors are immune to electromagnetic interference, they enable the multiplexed detection of an analyte, and without labels they do not affect the sample per se (Guo 2012). These characteristics make the optical biosensor a considerable option in various areas from drug research and environmental safety to food industry and clinical diagnostics to construct a highly sensitive, relatively inexpensive, and rapid detection system for the quantitative and qualitative data of molecular interaction (Homola 2008). The flexible and effective use of optical biosensors requires biological, chemical, and physical knowledge about the design and function of the optical biosensing surfaces and instrumentation. The following sections present the operation principle, the general definitions, and the basic assay formats related to optical biosensors. They also introduce different approaches to biofunctionalize the sensing surface and to prevent the non-specific adsorption of proteins (i.e. fouling). Furthermore, the end of this chapter describes the essential binding kinetics and thermodynamics of ligand – analyte interactions.

2.1.1 Operation principle and definitions

A biosensor is an analytical device that produces quantitative or semi-quantitative information about a specific ligand – analyte interaction (Thévenot *et al.* 2001). It integrates a biological recognition element i.e. ligand, such as antibody, into direct contact with a transducer. In the optical biosensor, the optical transducer converts the generated signal response of the biomolecule binding event to an optical format. The read-out and analysis of the optical signal is performed using a detector and a computer or an equivalent smart device.

The specificity and selectivity of a biosensing system rely correspondingly on the ability of the biological element to interact strongly with the analyte molecules, and to filter out the rest of the sample components without significant interaction (IUPAC 2014). When the ligand molecules are immobilized in direct contact with the surface of the transducer, the sensitivity can be determined as efficiency of the sensing system to generate a signal as a function of the concentration. The sensitivity of the sensing system is mainly dependent on the amount,

orientation, and affinity of the biological recognition element as well as on the performance of the transducer (Cooper 2002).

In practice, the non-specific binding between dissimilar and similar particles and surfaces masks the specific binding sites resulting in the loss of sensitivity in some extent. If the non-specifically and specifically binding particles accumulate and saturate the sensing surface, the upper limit of the dynamic range is reached and the sensing surface needs to be regenerated to recover the binding ability of the biosensor. The dynamic range is specified as a range of concentration that can be quantified reliably (IUPAC 2014). The resolution of the sensing system designates the limit for the statistical distinction between two measurement points.

According to the IUPAC definition (IUPAC 2014), the instrumental noise is an irregular fluctuation in the signal, which originates from the instrumentation of a biosensor. The baseline (or background) of the measurement, which is affected by the experiment conditions, the assay design, and the instrumental noise, is quantified by measuring a blank solution i.e. sample solution without the analyte of interest. The limit of detection (LOD) can be derived from the baseline by multiplying the standard deviation of the baseline signal by three.

From the statistical point of view, the repeatability is the closeness of independently measured results produced by the same operator for the same sample using an identical apparatus under the same experiment conditions after a short interval of time. The reproducibility is an external complement to the repeatability: the measurements are conducted for the same sample with the same method, but the operator, apparatus, and laboratory are different. (IUPAC 2014)

2.1.2 Assay formats

The biosensing surfaces can be designed by applying different basic approaches with general benefits and disadvantages. The simplest approach is the direct assay, where the ligand molecules are immobilized on the sensor surface and then the analyte molecules are incubated with the ligand or they are introduced on the surface in the flow buffer (Schasfoort 2017). The signal response is directly proportional to the concentration of the analyte. Additional features, such as regeneration ability, can be achieved by adding mediator molecules showing irreversible affinity of binding.

In some cases, when the immobilization of the ligand is challenging e.g. due to the deactivation of the ligand or the steric hindrance of analyte binding sites, one can switch the roles of the

ligand and the analyte to construct an inhibition assay (Helmerhorst *et al.* 2012). The analyte molecules are immobilized on the surface, and a sample solution containing an unknown amount of analyte is mixed with a suitable amount of ligand (Schasfoort 2017). During the introduction of the sample mixture, the surface-attached analyte molecules and free analyte molecules of the sample solution compete from the binding sites of the ligand molecules. Therefore, the signal response is inversely related to the concentration of the analyte (indirect assay). In other words, the low concentrations of the analyte in the sample results in a high signal response, and *vice versa*.

When the analyte has a small MW and does not generate a signal high enough, as is often the case for the sulfonamide inhibitors, a competitive assay may provide a solution. The sample solution containing the analyte is mixed with a specific amount of label-conjugated analyte, and the signal is generated when the label-conjugated and original analyte molecules in the sample solution compete for the binding sites of the surface-bound ligands. The signal response is inversely proportional to the concentration of the analyte. In optical biosensors, the label should have detectable intrinsic (e.g. high refractive index, RI; or MW) or inducible (e.g. fluorescence) properties (Guo 2012).

If the competitive assay does not alleviate the problem with signal level, one can construct a sandwich assay, where the generated signal coming from a direct assay is amplified for instance using gold nanoparticle- or latex particle-conjugated antibodies (Schasfoort 2017). The latter solution is a microfluidic version for the traditional enzyme-linked immunosorbent assay (ELISA) format (Weng *et al.* 2016). The addition of an amplifier in SPR applications may complicate the data analysis and sometimes result in false negatives, but it may also increase the sensitivity and lower the limit of detection, which is essential when analytes are measured in complex matrices at extremely low concentrations (Mariani and Minunni 2014). It is worth to notice, however, that bulky molecules lead to a more unstable sensing surface, and in optical methods, where an evanescent field is present, they also lower the sensitivity of the biosensing system

2.1.3 Biofunctionalization

The main advantage of biosensors is the use of a biological recognition element (i.e. ligand) that mimics the natural binding mechanisms usually with high affinity and specificity. This enables the determination of the biological activity using interaction kinetics. The sensing surfaces can be biofunctionalized by immobilizing ligands directly, or via a linker (e.g. His-tag) or mediator molecules (e.g. avidin protein) on the transducer surface (Homola 2008). The immobilization of ligands can also be performed for example on a two-dimensional planar surface (e.g. a self-assembled monolayer i.e. SAM deposited onto the transducer surface) or into a three-dimensional hydrogel (e.g. carboxymethylated dextran i.e. CMD).

SAM layers increase the degrees of freedom of a ligand, which correspondingly increase the probability of analyte binding (Mariani and Minunni 2014). In the case of commonly used mercaptoalkyls, the defects on a transducer surface affect the deposition of SAM surfaces, and they may cause local non-specific binding (shown in step 1 of Figure 1), or the deactivation of otherwise active and well-oriented ligand molecules (Schasfoort 2017). One alternative to alleviate this problem was seen in the article published by Zauner *et al.* in 2016, where the terminal ends of long-chain mercaptoalkyls had been linked to polyethylene glycol chains to smooth the sample solution-contacting surface.

Three-dimensional hydrogels provide significantly higher ligand density for the immobilization than two-dimensional sensing surfaces, where the ligand density is restricted to a maximum of one monolayer (roughly 1-2 ng mm^{-2}) (Schasfoort 2017). Furthermore, they provide protection against air bubbles and contaminants. Thick matrices may, however, distort the observed dissociation rate of an analyte as rebinding and diffusion-limited kinetics of the analyte may occur (Schasfoort 2017). Additionally, the excessive activation of carboxylated polysaccharides, such as CMD, by a frequently used non-specific EDC/NHS amine coupling chemistry may damage or prevent analyte binding by matrix crosslinking as well as increase the hydrophobicity of the matrix too much and precipitate the immobilized proteins. EDC and NHS are commonly used abbreviations for N-(3-dimethylaminopropyl)-N′-ethylcarbodiimide hydrochloride and N-hydroxysuccinimide, respectively.

The optimal performance of the sensing system in terms of sensitivity and reliability is achieved when the ligand molecules are immobilized homogeneously in an oriented-fashion at suitable surface density with stable immobilization chemistry that does not affect the activity or conformation of ligand molecules (presented in the left side of Figure 1) (Guo 2012; Trilling *et al.* 2013). In the real world, instability, miss-folding, cross-linking (step 4 in Figure 1), and non-specific binding of the ligand (step 3) as well as the imperfections of the immobilization matrix or surface, poor selectivity of the immobilization chemistry (step 2), and competing or interfering molecules (step 1), to mention but a few, lead to a notably lower sensitivity of the sensing system.

The immobilization methods of ligands and mediator molecules include entrapment and adsorptive immobilization as well as affinity binding and covalent coupling (Brena *et al.* 2013). In the entrapment method, the ligand molecules are permanently included into a polymeric network called matrix with non-covalent bonds, but the analyte molecules are free to enter and exit this matrix. The ligand leakage from the matrix may, however, compromise the reliability and operating time of such sensing surface.

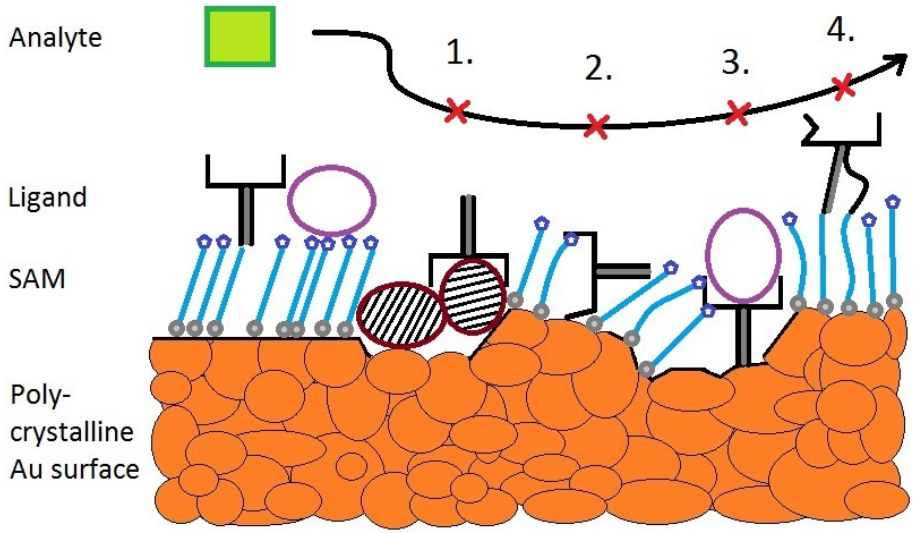

Figure 1. Schematic illustration of a truthful sensing surface. The analyte molecule may diffuse near the well-oriented and active ligand, and pass over the ligand molecules that are adsorbed non-specifically either to competing molecules, such as protein clusters (1) or the hydrophobic parts of SAM components (2). Additionally, the analyte molecule is not able to interact with a blocked binding site of the ligand molecules (3) as well as with the misfolded or denatured ligand molecules (4). The gold-facing thiol groups and hydrophilic head groups of the SAM are illustrated with grey and purple dots, respectively. The figure was recreated based on the illustration presented by Choi and Chae in 2010. The figure is not in scale.

Adsorbed ligand molecules are in turn immobilized non-specifically on the sensing surface by hydrogen bonding, van der Waals forces, ionic binding, and entropy-driven hydrophobic interactions (Schasfoort 2017). The drawbacks of this simple immobilization method are that non-specifically immobilized ligands compete with the non-specifically binding contaminants from the interactions with the sensing surface, and less than 10% of the immobilized ligand is in the active state as well as available for the interaction with the analyte.

The well-defined and specific affinity binding of complementary mediators can be utilized to immobilize ligands in a reproducible and efficient way. This method is, however, expensive and requires more expertise and optimization from the operator. (Schasfoort 2017)

The covalent immobilization enables the stable binding of ligands on a planar surface or into a three-dimensional matrix either with a specific or non-specific interaction (Homola 2008). There are numerous immobilization chemistries available for the different functional groups, such as thiols, amines, and aldehydes. The main challenges with the covalent immobilization arise when the optimization of immobilization conditions including the surface chemistry of the immobilization surface or matrix, the concentration of the ligand, and the reaction time of reagents, is required. The goal is to achieve a homogeneous sensing surface with a sufficient amount of active ligands at the same time preserving steric accessibility. The conjunction of protein-resistant surface designs with the covalent coupling of ligands may be complicated due the steric repulsion between the surface and ligand.

One strength of the reversible immobilization is the opportunity to regenerate the sensing surface when necessary by alternating the ambient conditions, such as temperature, ionic strength, pH, or polarity of the solvent, and reconstructing the sensing surface with a fresh ligand (Brena *et al.* 2013). This reduces the cost per analysis and enables the evaluation of sensor-specific repeatability of measurements. Zauner *et al.* presented in 2016 a versatile approach, where a genetically engineered version of avidin and a biotinylated immunoglobulin-binding protein (protein G) was utilized to construct a regenerative immunosensing platform without the use of harsh regeneration treatments. It has the capability to change specificity of the sensing surface or to remove all the proteins from the sensing surface depending on the use of two distinct regeneration solutions.

Tetrameric avidin and streptavidin molecules from chicken and *Streptomyces avidinii*, respectively, have been utilized broadly in the field of biomedicine, biotechnology, and biosensing owing to the formation of the extremely stable avidin-biotin complex ($K_D \approx 10^{-14} – 10^{-16}$ M), and the robust structure that tolerates extensive mutation (Laitinen *et al.* 2006). Avidin and streptavidin molecules have been placed in the role of mediator (Trilling *et al.* 2013) and ligand with pronounced performance. The development of the biotin-avidin technology by rational protein engineering has produced novel mutants of avidin and streptavidin with tailor-made properties, such as neutralized surface charges and reversible binding (Laitinen *et al.* 2006). For example, switchavidin (avidin with five specific mutations) shows ultralow non-specific binding of proteins owing to the neutral isoelectric point (pI). It also enables the breakdown of specific interactions with biotin molecules using rapid (less than 10 min) and efficient chemical treatment (Pollheimer *et al.* 2013).

2.1.4 Anti-fouling ability of biosensing surface

The decrease in the non-specific adsorption of sample components contributes positively to the sensitivity and reliability (lower number of false positives) of the biosensing system. The sample solution may contain amphiphilic proteins and peptides, water-soluble carbohydrates, and hydrophobic lipids in different combined forms e.g. in vesicles with integral proteins (Nallani *et al.* 2011). Consequently, the adsorption behavior of complex media may differ significantly from the adsorption behavior observed for the single biomolecule solutions, and the discussion of this section is limited to the non-specific adsorption of proteins i.e. to the fouling (Vaisocherová *et al.* 2015). The main challenge is to design an anti-fouling surface that enables the ligand molecules (mostly proteins) to be immobilized in an active state, but still rejects the non-specific adsorption of other protein components (Pop-Georgievski *et al.* 2013). The following paragraphs introduce some of the basic principles and factors affecting the protein adsorption phenomena, and the alternatives to improve the anti-fouling ability of biosensing surfaces.

Numerous adsorption models exist for proteins, but as a compressed version, the adsorption of proteins usually follows a dynamic process called Vroman effect, where the high mobility proteins adsorb first onto a surface, and then they are replaced by the lower mobility proteins that show higher affinity (Vaisocherová *et al.* 2015). Proteins roll, spread, diffuse laterally, form clusters, and change conformation on the sensing surface in order to find the lowest possible energy state together with neighboring molecules (Barnes and Gentle 2011).

Most important factors affecting the protein adsorption are the surface energy, polarity, charge, and morphology (Barnes and Gentle 2011). Additionally, post-translational modifications, such as lipids and sugar groups, artificial chemical modifications, such as biotin residues, and conformational changes may alter the expected adsorption behavior. The pI of proteins and the ambient pH of sample solution defines the nature of electrostatic interactions with charged particles or surfaces. For instance, a positively charged surface attracts negatively net charged proteins (pH > pI) on the surface and *vice versa.* When pH equals pI, the net charge of the protein is neutral and the impact of the hydrophobic interactions on the adsorption behavior is higher. In biosensing, the electrostatic adsorption of undesired proteins can be controlled in some extent by alternating the pH conditions (Schasfoort 2017) or increasing the ionic strength of the sample solutions (Barnes and Gentle 2011), but the main limiting factors e.g. in the bioassays come from the properties of present proteins (ligands, mediators, fouling proteins) as well as from the surface chemistry of the sensing platform.

The anti-fouling properties of the sensing surface are often evaluated using single protein solutions of HSA (or BSA), IgG, lysozyme, and fibrinogen (Vaisocherová *et al.* 2015). Fibrinogen is a relatively large (MW = 340 kDa) protein found from human blood-plasma and it adsorbs easily onto hydrophobic surfaces. Lysozyme, in turn, is a relatively small protein (MW = 14 kDa) with positive net charge at physiological conditions owing to a high pI (~12). It can be used to model the electrostatic adsorption of proteins onto surfaces.

Numerous shared physicochemical properties of protein-resistant surfaces have been found: hydrophilicity, electroneutrality, lacking hydrogen-bond donors, and having hydrogen-bond acceptors to mention but a few. Consequently, the immobilization of the ligand mainly via physical adsorption e.g. ionic and hydrophobic interactions are not suitable for applications, where low-fouling properties are required. The high surface density and highly ordered structure of SAMs as well as the hydrophilic interface with the sample solution enhance the anti-fouling ability of the sensing surface. Oligo (ethylene glycol)-terminated SAM surfaces are commonly used in preliminary studies of bioassay development as they perform well in single-protein solutions, but they do not show adequate anti-fouling properties in more complex media, such as blood serum. (Vaisocherová *et al.* 2015)

Traditionally, the anti-fouling property of sensing surfaces have been improved by acetylation or succinylation of protein ligands. The statistical nature of these chemical modifications, however, produces an over-acetylated fraction of protein with reduced stability (Taskinen *et al.* 2014). Genetic engineering has been used as an alternative to chemical modifications, ultimately leading to more defined surface chemistry without significant loss of stability or activity.

From the biosensing surface point of view, the anti-fouling properties of a sensing surface can be sometimes improved by blocking the surface, e.g. with BSA. The efficiency of this approach is based on the dense monolayer of a low mobility protein that can resist the adsorption of protein clusters (Rabe *et al.* 2011). However, the BSA blocking may result in the blockage of analyte entrance to the binding site of a ligand, and lower the sensitivity of sensing surface (presented in the step 3 of Figure 1). Furthermore, the BSA blocking layer, even a dense layer, may lack the capability to resist the penetration and spreading of protein clusters if the BSA blocking layer is deposited onto a too hydrophobic surface, or if there are surface defects on the gold layer (step 1 of Figure 1). This may lead to false negative or ambiguous responses, which are notably common challenges in the field of assay technology.

As an alternative to the BSA blocking, one can add a protective barrier, such as a thick hydrogel or polymeric mesh, which prevents undesired sample components from protruding into the sensitive volume of the sensing surface (i.e. the volume where the evanescent field of SPR extends) (Schasfoort 2017). Bio-inert hydrogels lower the fouling levels also by electrostatic repulsion, when protein molecules approach the hydrogel and compress the equal-charges along the polymer chains. On the other hand, the protective barriers may lead to the mass transport limitation (MTL) of the analyte (described in section.

It is also worth mentioning that the flow systems are better than the steady-state systems to avoid the non-specific adsorption of biomolecules (Schasfoort 2017). The contact time of sample solution with the sensing surface is shorter, which favors high affinity (fast association; high stability of ligand-analyte complex) interactions over low affinity (slow association; low stability of ligand-analyte complex) interactions.

2.1.5 Interaction kinetics

The pharmacodynamic and pathological knowledge related to drug development and disease progression have been strong driving forces to develop fine-tuned instrumentations and analysis software for the measurement of interaction kinetics. In the first mentioned area, the kinetic measurements provide information on the formation speed and stability of the drug-target complex as well as a rough estimation for the effective dose of a drug. These factors can be in turn applied in the lead optimization process (Cooper 2002). In the second area, the affinity constant together with association and dissociation rate constants can explain for instance the rapid course of a disease as well as the resistance to drug therapy (Rutgers *et al.* 2000). The traditional way to solve only affinity between interacting molecules does not provide the whole picture. Figure 2 demonstrates how the same affinity values of different analytes may hide totally different kinetic profiles of the interaction. Notably, the equilibrium binding analysis of the interactions, however, supports the calculation of kinetic values.

The ligand – analyte interaction kinetics consists of three steps (exemplified with the red kinetic curve in Figure 2): (1) an association phase, where analytes bind to the available binding sites of ligand molecules; (2) an equilibrium phase, where the rates of binding and dissociation are equal; and (3) a dissociation phase, where buffer flow has replaced the analyte solution, and the analyte molecules leave the binding sites of ligand molecules.

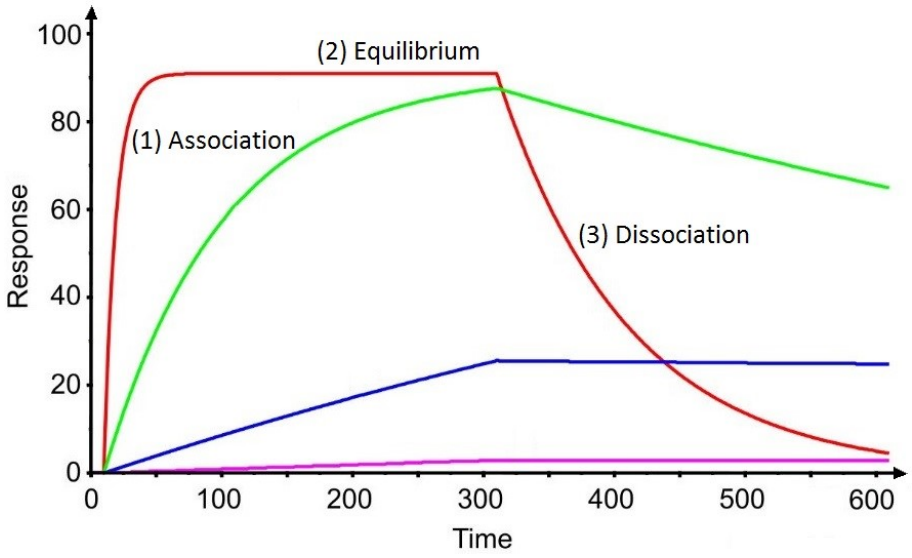

Figure 2. The kinetic profiles for four analytes. They all have the same affinity with the ligand, but they show distinct velocities of (1) association and (3) dissociation (exemplified with the red kinetic curve). In the (2) equilibrium phase, the association and dissociation processes are in balance. The figure was recreated based on the plot presented in www.sprpages.nl/sensorgram-tutorial/a-curve; August 20, 2017.

When an increase in the analyte concentration does not generate any higher signal, the saturation point of the interaction is reached. If the buffer flow is incapable of removing analyte molecules from the binding sites of ligands i.e. the stability of ligand-analyte complex (k_d) is practically too high for the serial injections of the analyte dilutions, a regeneration step (not shown in Figure 2) can be applied (Cooper 2002).

The affinity between ligand and analyte molecules can be seen either thermodynamically as a transfer of heat and entropy, by the mass law as a movement and fusion of individual molecules or kinetically as a relation of dissociation (k_d) and association (k_a) rate constants, when the saturation of the interaction has not started (Figure 3).

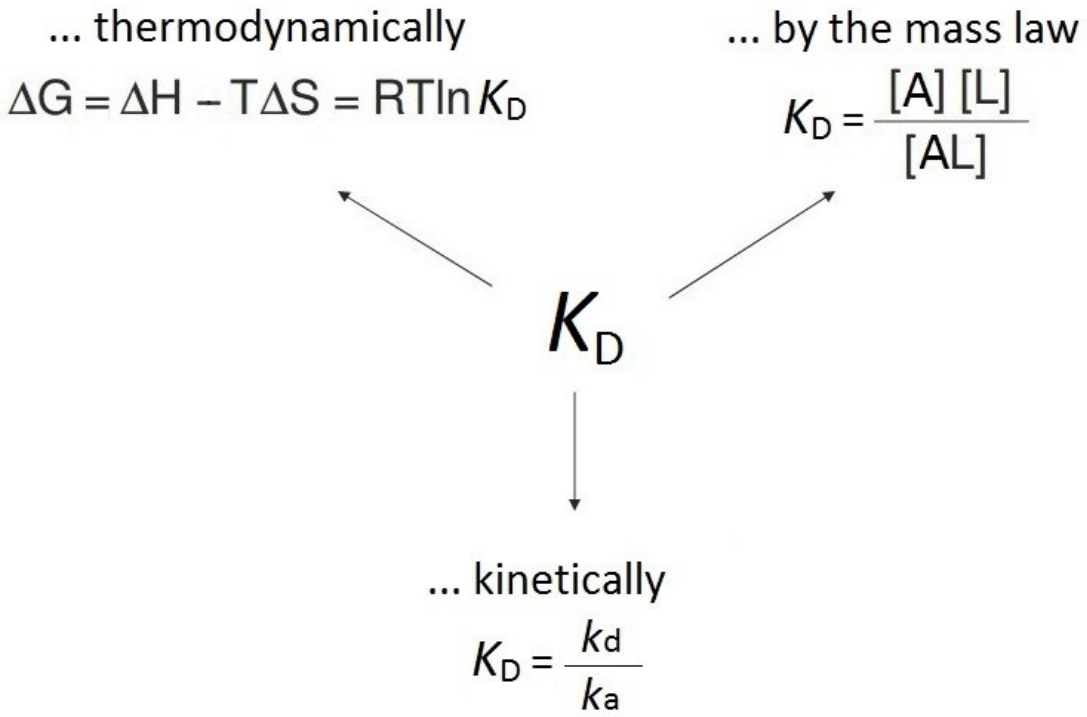

Figure 3. Thermodynamic, mass law-based, and kinetic viewpoint on the affinity of a ligand – analyte interaction. In the kinetic expression, the dissociation constant (K_D; the reciprocal of the association constant K_A) is the quotient of k_d and k_a are the dissociation and association rate constants of the interaction. For the thermodynamic expression of dissociation, G is Gibbs free energy, H is enthalpy, and S is entropy. T is the ambient temperature and R is the ideal gas constant. [L], [A], and [LA] denote the concentrations of ligand, analyte, and ligand-analyte complex, respectively. The figure was recreated based on the presentation of Martin Vogtherr, Ph.D. (AstraZeneca, currently in Merck). The presentation named "NMR to characterise protein-ligand interaction: Applications in drug discovery" was retrieved in August 19, 2017.

The kinetic analysis can be performed in principle for the dataset that includes a series of analyte dilutions covering a range correlating with 0.1 and 10 times the K_D value. The analyte dilutions are injected in a row with an expected dissociation time using air-bubble segmentation that prevents a diffusional dilution of sample with running buffer, and ensures the accurate concentrations of analyte molecules. Alternatively, when the dissociation rate constant (k_d) is sufficiently small, one can inject analyte dilutions without the dissociation phase, and determine dissociation rate constant from the tail part left after the injections. (Schasfoort 2017)

2.2 SPR biosensing

Surface plasmon resonance (SPR) biosensing systems have been designed for numerous analytes, such as for the lead molecules of drug discovery (Cooper 2002), for human cancer biomarkers (Mariani and Minunni 2014), and for mycotoxins in the food industry (Li *et al.* 2012). The properties and the number of samples as well as the application area and the purpose of measurement set some requirements for the instrument and the sensing surface design. The deep understanding of these requirements is essential for the planning and optimization of the experiments. The next sections describe the essential theory behind the SPR phenomenon, present the structure of basic SPR instrumentation, and list some of the most common challenges faced by the SPR biosensors.

2.2.1 Fundamental theory of the SPR phenomenon

Surface plasmon resonance is defined in various ways in the literature, but essentially SPR is composed of propagating electron density waves called surface plasmons (SPs). SPs occur at the interface between a metal and a dielectric, where free electrons (signified by the negative dielectric constant of the metal) are able to oscillate under certain conditions (Couture *et al.* 2013). More precisely, the excitation of SPR requires a functional combination of the optical and physical properties of the metal and the dielectric layers (RIs, dielectric constants, and thicknesses) as well as the right wavelength and polarization of laser light in addition to a suitable incident angle of laser light (Homola 2008). When the optical properties of the dielectric layer alter e.g. due to the biomolecule adsorption, the conditions where the propagating electron density wave is excited, change accordingly. The wavelength of laser light defines the propagation length of SPR from the gold surface that is sensitive to the optical changes. The incident laser light must be p-polarized because only p-polarized light can induce

SPs. The evanescent field of SPR is directed perpendicular to the interface between a metal and dielectric in both directions as shown in the inset of Figure 4.

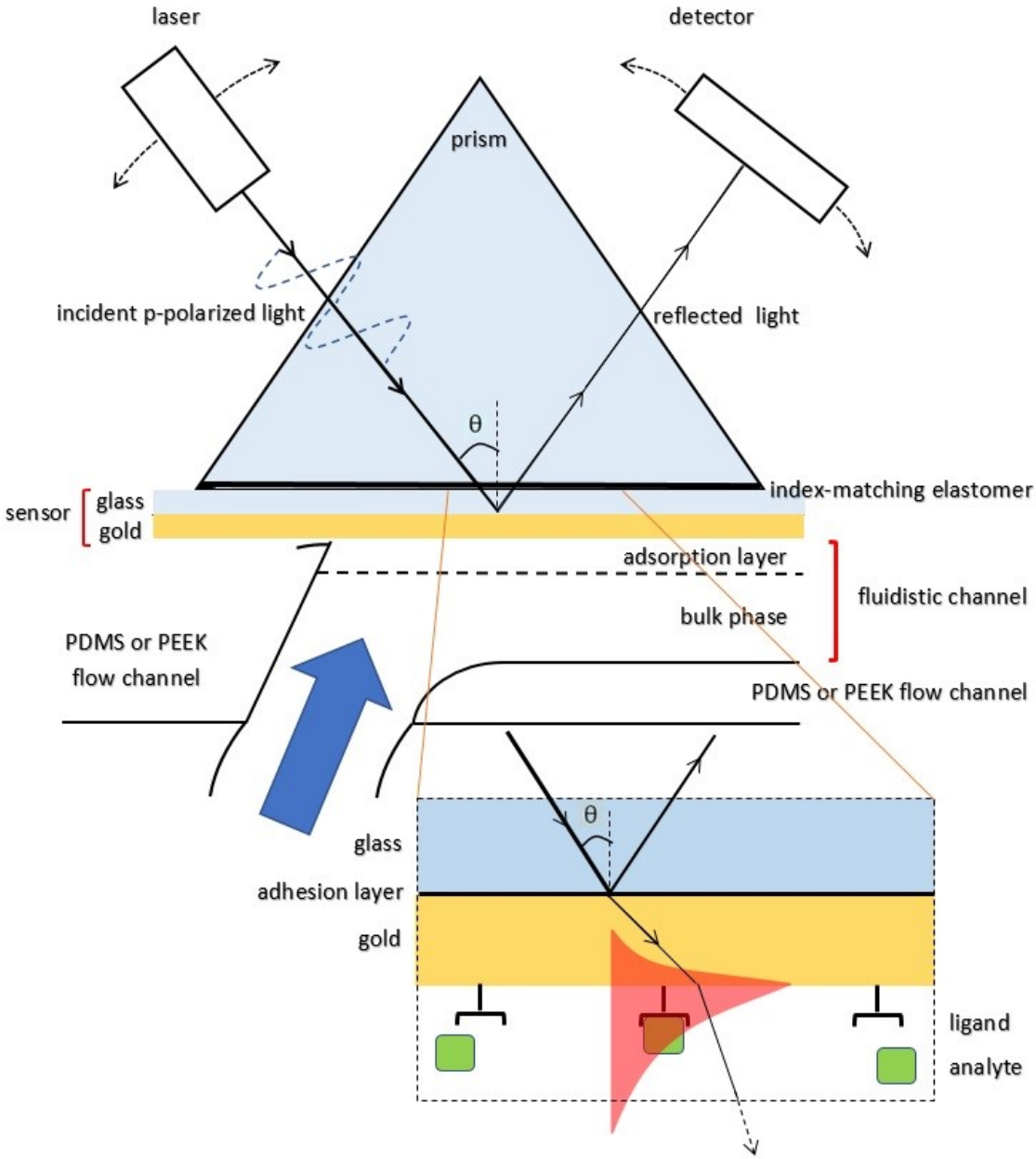

Figure 4. SPR detection system based on Kretschmann-Raether configuration. The presented parts from the MP-SPR Navi™ instrumentation cover the flow cell made of PDMS or PEEK polymers; the fluidic channel, which is formed when the flow channel cuvette is docked against the sensor slide; and the prism as well as the moving laser (or equivalent) and detector. The prism is in optical contact with the gold layer via index-matching elastomer (Kretschmann-Raether configuration). The schematic inset demonstrates the reflection (arrow upwards) and refraction (arrow downwards) of incident p-polarized laser light at the interface between the glass substrate and the gold layer as well as the induced evanescent field of SPR (marked with red area). The shape of the illustrated evanescent field represents the exponentially decaying magnitude of SPR) (Schasfoort 2017). Analyte molecules are injected into a fluidic channel, where they move into and away from the adsorption layer by diffusion and convection. The figure is not in scale.

The field intensity of the evanescent field decays exponentially and it is stronger close to the dielectric than the metal. The sensitivity of the SPR detection is limited to the physical distance (commonly referred to as a penetration depth) determined by the decay length of the evanescent wave. In practice, the decay length of the evanescent wave corresponds roughly to one third of the laser wavelength used in the instrumentation. This usually covers the absorption layer of biomolecules (presented in the inset of Figure 4) and makes traditional SPR a surface-sensitive technique.

The SPs can be excited in local and planar mode depending on the dimensions of the transducer material in relation to the wavelength of laser light. For example, nanoparticles (NPs) have significantly lower dimensions than the wavelength of laser light, which enables the excitation of strong, but not so far reaching SPs (Olaru *et al.* 2015). This phenomenon is commonly referred to localized SPR (LSPR). NPs can be utilized for instance in the amplification step of small molecule immunoassay. On a planar surface, the excitation of SPs is confined to a thin layer (semi-infinite) of the metal that provides a versatile platform for the integration of a fluidic system (Couture *et al.* 2013).

Traditional planar SPR can be put into practice either with a Kretschmann-Raether or an Otto configuration. In the first option, the metal layer is in contact with the prism, and in the second option, there is a small gap between the prism and the metal layer (Schasfoort 2017). The Otto configuration provides a steeper profile of the SPR peak than the Kretschmann-Raether configuration, and therefore, it enables higher angular resolution to the SPR peak minimum angle shift. Due to practical challenges related to the docking of the sensor with a small gap, the Kretschmann-Raether configuration is a more popular approach at least among the commercial instruments (Couture *et al.* 2013). Therefore, later discussion regarding the SPR detection systems is limited to the planar Kretschmann-Raether configuration.

2.2.2 MP-SPR instrumentation

The Kretschmann configuration-based optical detection system of SPR with a flow cell cuvette-based fluidic system (presented in Figure 4) includes a laser that emits p-polarized light at a convenient wavelength, a prism that couples the laser light on the gold surface of a sensor slide, and a detector that records the intensity of reflected laser light (Couture *et al.* 2013). In the optical setup of the MP-SPR Navi™ instrument manufactured by BioNavis Ltd (Tampere, Finland), the laser system and the detector are in a synchronized movement that

enables a broad angular scan of incident angles with corresponding intensity. The information-rich measurement data can be plotted in a full SPR curve (presented in Figure 5).

The sensor slide that is used as a transducer forms the interface for the electron oscillations of the SPR phenomenon described in the previous section. The standard gold sensor slide of MP-SPR Navi™ instruments (BioNavis Ltd) comprises the following layers listed from the prism side to the sensing interface: (1) a glass substrate, (2) a thin adhesion layer, and (3) an approximately 50 nm thick "plasmonic" layer of planar gold as depicted in the inset of Figure 4. The glass substrate makes the sensor slide tougher. A thin adhesion layer is applied on the glass substrate to improve the quality of plasmonic metal deposition (Sexton *et al.* 2008). Silver has better properties for the SPR excitation, but poor inertness (Olaru *et al.* 2015). Therefore, the second-best metal, gold, is most often chosen for the plasmonic metal layer. During the docking of the flow cell cuvette, the glass prism is fixed in optical contact with the glass substrate of the sensor slide via an index-matching elastomer or oil. At the same time, the fluidic channels of the flow channel are formed against the gold surface of the sensor slide.

The purpose of the flow cell is to direct the sample flow to the fluidic channel, where the analyte molecules move into and away from the adsorption layer by diffusion and convection. The flow cell is most often made of a polymeric material that shows chemical resistance and anti-fouling properties at some level. Polyether ether ketone (PEEK) and poly(dimethylsiloxane) (PDMS) polymers are commonly used flow cell materials (Schasfoort 2017).

When the laser light hits the interface between two media (as in the inset of Figure 5), there are four possible outcomes: the light is reflected from the interface, refracted at the interface, or absorbed or scattered by the media (not shown for clarity). These phenomena occur mostly at the same time and they are dependent on the incident angle of light, the RIs and absorbance of the media as well as the surface topography of the interphase (Cooper 2002; Schasfoort 2017).

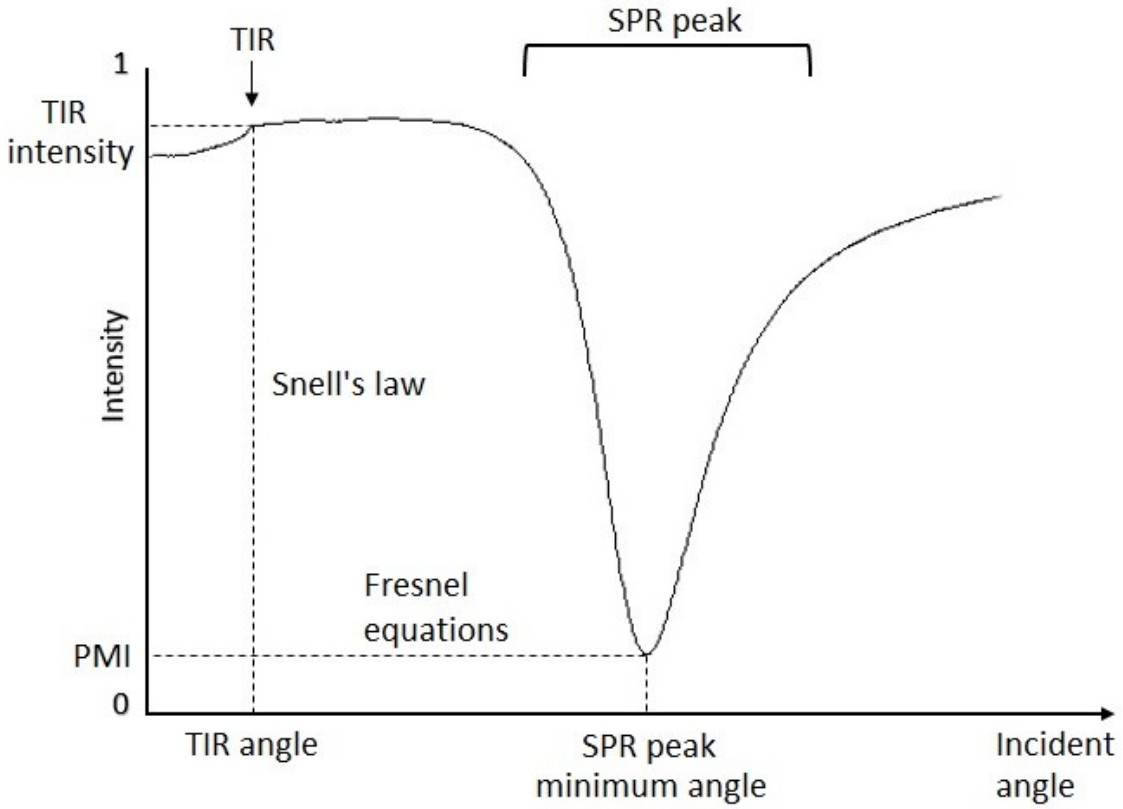

Figure 5. The full MP-SPR curve covering the SPR peak as well as the position of total internal reflection (TIR). The SPR peak minimum angle is the most utilized parameter, but the measurement of SPR peak minimum intensity (PMI) as well as the position of TIR enables the follow-up of optical scattering and absorbance properties of the dielectric layer as well as the compensation of bulk effects, respectively. The ratio of PMI and TIR intensity is described by Fresnell equations. The angle of TIR can be calculated using Snell's law. The MP-SPR curve was exported from MP-SPR Navi™ DataViewer software (BioNavis).

The MP-SPR Navi™ instruments measure a broad range of incident angles to monitor all the previously mentioned fates of laser light. At first the analyte molecules diffuse from the bulk phase to the adsorption layer. Then the interaction of the sensing surface-immobilized ligands with the analyte molecules changes the optical properties, such as the RI, near the sensing surface which induces a shift in the SPR peak minimum angle (denoted in Figure 5). Practically, the conversion of photons to plasmons can be seen as an intensity drop in the detector at a certain incident angle of laser light. There are a few instruments that follow shifts in the other optical parameters of the reflected light, such as phase (Huang *et al.* 2012), wavelength (Couture *et al.* 2013), and SPR peak minimum intensity (PMI) (Kurihara and Suzuki 2002) with pronounced benefits, but they have marginal commercial interest. For the same reason, these approaches are left outside this thesis.

Some samples absorb or scatter the laser light, e.g. NPs, which is detected as an increase in the PMI (Viitala *et al.* 2013). In this context, the optical scattering and absorptivity mean that less photons of laser light are capable of exciting SPs, and this is detected as increase in PMI. Snell's law provides the critical angle of total internal reflection (TIR) when the RIs of materials are

known (Couture *et al.* 2013; Schasfoort 2017). The TIR angle can be utilized to follow the beginning and the end of sample solution injection when the signal responses are small, as well as to compensate e.g. the buffer mismatch-caused bulk effect. Fresnel equations determine the ratio of refracted and reflected light, which can be applied when the thicknesses of multilayered structures are resolved (Nabok and Tsargorodskaya 2008).

The main advantages of the SPR systems in biosensing applications are the non-invasive optical detection and the calibration-free concentration analysis that is based on the natural occurrence of RI changes, when the ligand molecules adsorb on the sensing surface (Helmerhorst *et al.* 2012).

2.2.3 Challenges in SPR biosensing

Mass-transport-limited binding occurs when the diffusion of an analyte is slower than the association rate of the analyte on the sensing surface (Cooper 2002). It is characteristic especially for very large analytes (with low diffusion rates) as well as for the analytes showing extremely fast association kinetics (in comparison to the diffusion rate). MTL binding may also lead to the undesired re-binding of an analyte, which distorts the observed kinetics of the interaction (Papalia *et al.* 2006). In other words, the association and dissociation rates of the analyte molecule seem to be slower than they are in reality. MTL can be largely avoided by increasing the flow rate or lowering the ligand density on the sensing surface (Cooper 2002). In bioassays, where the concentration of an analyte is determined, the high ligand-density-induced MTL is, however, exploited as this makes the analyte binding process mass-transport-dependent, and less dependent on the ligand – analyte kinetics. The use of the MTL factor in the kinetic calculations is not recommended (only with troubled cases).

The RIs of buffers and sample materials are slightly temperature-dependent, which makes SPR detection systems susceptible to temperature-induced signal drift. This issue is handled with an accurate temperature controller that can efficiently increase and lower the flow cell temperature as well as with a parallel reference channel. The signal drifts and bulk effects originating from the swelling of a hydrogel matrix, or from the variation in mass distribution after ligand immobilization affect the quality of the measurement data. They can be treated with an extended stabilization time of the hydrogel matrix in the running buffer as well as with a proper reference channel subtraction. (Cooper 2002)

Small MW analytes are regularly prepared and stored in 1-10 % dimethyl sulfoxide (DMSO), a highly polar solvent that is a gold standard for the solubility enhancement in the lead molecule generation of drug discovery. In the case of hydrogel matrices, the use of DMSO may, however, cause a bulk effect that masks the specific binding signal of an analyte (Cooper 2002). When the ligand molecules are immobilized into the hydrogel matrix, variation in the hydrogel void volume (i.e. the volume occupied by macromolecules and not available for the analyte molecules) arises between the active and reference channel. One way to circumvent this problem (sometimes called the excluded volume effect) is to create a calibration curve for the suitable range of DMSO concentration in running buffer without the analyte molecules (Frostell-Karlsson *et al.* 2000). This treatment 'normalizes' the bulk RI changes observed in the different flow cells.

Finally, the air bubble management is crucial for the success and reliability of the ligand immobilization and subsequent experiments with an analyte. Air bubbles prevent molecules from adsorbing and they may cause long-lasting displacements in the signal response if they remain on the surface (Biacore^{TM} Assay Handbook 2012). The buildup and movement of air bubbles on the sensing surface increase the light scattering and change the RI of the sample solution, respectively (Vallée *et al.* 2005). Practically, these processes can be monitored as an increase in the PMI signal and as spikes in the SPR peak minimum angle signal, respectively, to assess the reliability of measurement results (Biacore^{TM} Assay Handbook 2012). The formation of air bubbles can be reduced by degassing the buffers and samples by sonication in an ultrasonic water bath as well as stirring under vacuum.

3 OBJECTIVES

The two primary aims of this thesis were to adapt the protocols introduced by Zauner and collaborators in 2016 to a two-channel MP-SPR instrument manufactured by BioNavis Ltd, and to assess the performance of the regenerable biosensing system. In addition, it was interesting to explore if the real-time measurement of the full SPR curve and the TIR angle and intensity would reveal something new about the binding event of multivalent proteins.

The secondary aim was to evaluate how a four-channel MP-SPR prototype of BioNavis company adjusts to the challenges commonly faced by the optical techniques when rapid association kinetics of small MW drugs are measured in an angular scan mode. The broadly cited article of Papalia *et al.* 2006 was selected as a reference article, owing to the comparable instrumentation (a four-channel Biacore™ 3000 SPR instrument from GE Healthcare) and the well-documented protocol that can be applied to the instrument testing of kinetic limits. The human carbonic anhydrase II (hCAII) enzyme was selected instead of bovine carbonic anhydrase II for the experiments as this resembles more closely the pharmacodynamics of human-targeted drugs.

4 MATERIALS AND METHODS

4.1 Immunosensing platform with stepwise regeneration

4.1.1 Materials

The running buffer, phosphate buffered saline (PBS) pH 7.30 containing 1.8 mM KH_2PO_4, 10 mM Na_2HPO_4, 140 mM NaCl, and 2.7 mM KCl was prepared by dissolving corresponding amounts of salts in deionized water (approx. 18.2 MΩ cm) and adjusting the pH of the running buffer with concentrated HCl. All the buffer components were purchased from Merck (Darmstadt, Germany). At the end, the running buffer was filtered through a sterile Nalgene® bottle-top filter (pore size 0.45 µm; Sigma-Aldrich, Saint Louis, MO, USA), autoclaved in-house, and stored at +4 °C for few weeks at maximum.

The b-SAM was deposited on the gold surface of a standard MP-SPR Navi™ sensor slide (BioNavis) with some changes to the original protocol described elsewhere (Pollheimer *et al.* 2013. Supporting Information p. 19 - 22). The b-SAM membrane was prepared from matrix alkanethiols, MAT (HS-C_{11}-$(EG)_3$-OH; MW = 336.53 g mol^{-1}; ProChimia Surfaces) and biotin-terminated alkanethiols, BAT (HS-C_{11}-$(EG)_6$-Biotin; MW = 694 g mol^{-1}; ProChimia Surfaces, Sopot, Poland) by Martin Albers from BioNavis company. Briefly, chloroform dissolved MAT and BAT were mixed at a molar ratio of 80/20 to gain the desired biotin content of b-SAM surface. Prior the deposition, the gold sensor slides were cleaned with boiling ammonium peroxide solution (deionized water, 30 % hydrogen peroxide and 30 % ammonium hydroxide at volumetric fractions 5/1/1, respectively) for 3 minutes and rinsed multiple times with deionized water and 95.5 wt% ethanol (Altia Industrial, Rajamäki, Finland). Sensor slides were placed in Petri dishes with 10 mL ethanol and 0.5 mL of the mixture was applied into ethanol by pipetting with gentle mixing done with the tip. The Petri dishes were enclosed with aluminum foil to prevent the evaporation of ethanol. After overnight deposition at room temperature (RT), the sensor slides were washed with ethanol and dried with nitrogen gas. The sensor slides were stored at +4 °C and before use they were stabilized at 20 µl min^{-1} running buffer flow. It was possible to re-use the sensor slides after the experiments for some weeks. The fully regenerated sensor slides were rinsed multiple times with deionized water, blown dry with compressed air, and stored at +4 °C.

The protein solutions were used as received and diluted directly in the running buffer or the sample buffer. The protein concentrations of immobilization solutions were confirmed at 280 nm wavelength by a NanoDrop 2000 ultraviolet – visible light (UV-Vis) spectrophotometer (Thermo Fisher Scientific, Waltham, MA, USA). The purity of proteins was assessed based on the absorbance ratio A280/260 in addition to the information reported in the certificate of analysis or the specification of the protein sample. The salt or preservative residuals of lyophilized proteins or protein stock solutions were ignored in the protein concentration determination, and prospective bulk effects were accepted due to the low concentrations.

The immobilization solution of switchavidin was prepared from a lyophilized and -20 ºC stored protein aliquot that was produced, purified, and characterized by Niklas Kähkönen from the Protein Dynamics research group. The theoretical MW of tetrameric switchavidin is 57.2 kDa (Taskinen *et al.* 2014. Figure S2). The optical extinction coefficient, κ (i.e. how much light at a given wavelength is absorbed into a protein solution of a given concentration) had been calculated earlier at 280 nm in water using a ProtParam tool (Gasteiger *et al.* 2005) resulting in 23615 M^{-1} cm^{-1} (http://biomeditech.fi/Protein_Shop/switchavidin.html; March 24, 2017). The integrity and purity of non-protein contaminants had been tested with a SDS-PAGE method and an UV-Vis spectrophotometer.

The net surface charge of switchavidin had been neutralized by genetic engineering to improve the anti-fouling feature against counter-charged molecules (Taskinen *et al.* 2014). In detail, three neutralizing mutations (K9E, R124H, and K127E) that do not interfere with the ligand binding or structural integrity of the tetramer had been designed and introduced to a M96H/R114L mutant form of avidin that show improved affinity towards the conjugated biotin and controlled regeneration of biotin-avidin-biotin bridges (Taskinen *et al.* 2014). The resulting isoelectric point (pI) of switchavidin is 7.02.

Lysozyme enzyme (from chicken egg white; dialyzed) and bovine serum albumin (BSA; heat shock fraction; ≥ 98 %) were purchased in the form of lyophilized powder from Sigma-Aldrich. The whole IgG purified from normal human serum (h-IgG) by affinity immunoelectrophoresis was purchased in a storage buffer from Jackson ImmunoResearch (West Grove, PA, USA).

The (biotinylated) immunoglobulin-binding protein originally expressed in Streptococci (group G) and now termed “biotinylated protein G” was utilized as a mediator to immobilize IgG molecules on the switchavidin layer. The truncated form of the (biotinylated) protein G

lacking the Fab and albumin binding sites, and the membrane-binding regions was purchased in the form of lyophilized powder (≥ 98 % by Biuret assay) from Sigma-Aldrich. A single protein G molecule had been biotinylated with three biotin residues on average according to the certificate of analysis.

The sensing platform was biofunctionalized using monoclonal human prostate-specific antigen (PSA) targeting IgG antibodies (anti-PSA; ≥ 95 %; Medix Biochemica, Espoo, Finland). The dilution series of anti-PSA (nominally 200 nM, 100 nM, 67 nM, etc. down to 0.02 nM) were prepared from a 670-nM stock solution with sample buffer that was running buffer with additional 1 μM of BSA (Sigma-Aldrich).

The solution used for normal regeneration was prepared by dissolving 100 mM glycine (≥ 98 %; VWR International, Radnor, PA, USA) in deionized water and adjusting pH to 2.7. The solution for rigorous regeneration was prepared by dissolving 0.25 % of sodium dodecyl sulfate (SDS, 99.8 %; VWR International) in deionized water, adding 2.5 % citric acid (99.7 %; VWR International) and adjusting pH to 2.0. The simple washing solution for protein residuals was prepared by dissolving 0.5 % of SDS (VWR International) in deionized water.

4.1.2 SPR experiments

The SPR measurements were performed using MP-SPR Navi™ 210A VASA instrument (BioNavis) equipped with a standard PEEK flow cell that forms two fluidic channels over the sensor surface. The samples were loaded into the fluidic system of the instrument from preset vials with autosampler-controlled air-bubble segmentation to ensure accurate concentration of sample molecules. The SPR data was recorded simultaneously from the measurement spots of two flow channels, which were covered with differing protein assemblies depending on the experiment. The SPR instrumentation contained four lasers measuring at two different wavelengths (670 nm and 785 nm) in each flow channel. The running buffer and reagents were equilibrated at RT approximately for 15 minutes (some millilitres) to one hour (hundreds of millilitres), and degassed before use by tapping the liquid filled plastic syringe under negative pressure. All the measurements were performed at 25 ºC using a 20 μL min^{-1} flow rate unless otherwise noted.

The regeneration of sensor slides was performed by removing the switchavidin layer and the proteins bound on top of it (termed as “rigorous regeneration”) with a 12-min injection of 2.5 % citric acid (pH 2.0) and 0.25 % SDS. The subunits of switchavidin dissociate and denature, and

after the removal of tiny protein remnants by an 8-min injection of 0.5 % of SDS, the sensor slide is ready for the new cycle (Pollheimer *et al.* 2013).

Stability of the instrument and b-SAM

Prior the SPR experiments, the running buffer was filtered through a Millex®-VV sterile syringe filter (Merck Millipore, Billerica, MA, USA), which was equipped with a 0.1 µm pore sized hydrophilic PVDF membrane to sterilize aqueous solutions. At the beginning of the experiments, the flow cell was primed with b-SAM deposited gold sensor and filled with the running buffer using 100 µL min^{-1} flow rate. This was verified by a single angular scan of the SPR peak minimum as air bubbles can be detected as peaks in the region of 42 – 45 degrees. Then, the injection system was cleaned with two 5-min injections of 1% Hellmanex III (Hellma Analytics, Müllheim, Germany) with short buffer injections between. In the next step, a full SPR curve was measured at 20 µL min^{-1} flow rate exceptionally at +20 °C. The subsequent measurements were performed with higher flow cell temperature (+25 °C) than ambient temperature in order to reduce air bubble formation. The baseline drift was calculated manually from the linear regression of a 30-minute time period. The additional requirements were the stabilized flow cell temperature and PMI signal that indicates the buildup of air. Randomly occurring peaks with the magnitude higher than the noise level times two (illustrated in Figure 6) were excluded from the signal analysis. The definition of randomly occurring negligible peaks is based on the assumption that two standard deviations of the signal cover 95.5 % of random variation (~ i.e. noise) in the signal (Armbruster and Pry 2008). The average drift and sample standard deviations were reported separately for the upper and lower flow channel.

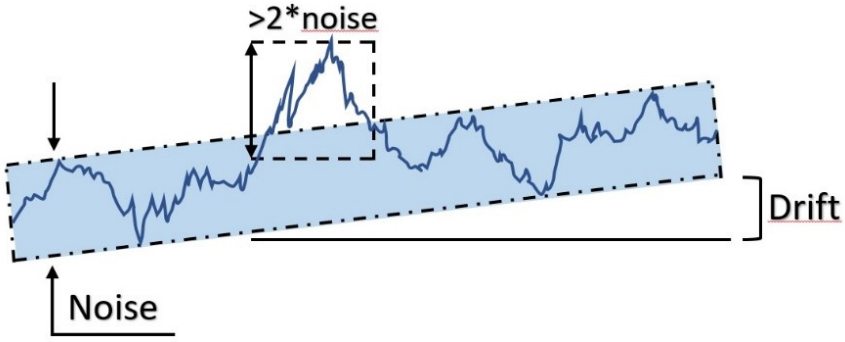

Figure 6. A schematic illustration of noise, drift, and a peak with magnitude higher than the noise level times two. The figure was recreated based on the illustration presented at http://hplc.chem.shu.edu/NEW/HPLC_Book/Detectors/det_nise.html in August 22, 2017.

Switchavidin immobilization on the biotinylated gold surface

Switchavidin was immobilized on the biotinylated gold surface at 2 μM concentration by a 10-min parallel or serial injection. The switchavidin immobilization solution was degassed under vacuum before the injection to minimize air bubble formation. The arithmetic mean of switchavidin immobilization levels was reported with sample standard deviations (SD).

Anti-fouling ability of the switchavidin surface

The anti-fouling ability of the switchavidin layer and the hydrophilic b-SAM surface was evaluated against BSA, lysozyme and human immunoglobulin G (h-IgG) molecules that were introduced at a concentration of 1 mg mL^{-1} individually for 5 minutes. The fouling levels of double BSA-blocked and non-blocked switchavidin layers were recorded from separate flow channels, and compared to assess the efficiency of BSA blocking. The response level of the second BSA injection was compared with the fouling level of the first BSA injection to determine the completeness of BSA blocking process.

Biofunctionalization of biotinylated protein G layer with anti-PSA

At first, the reference flow channel was passivated with a 3-min injection of 2 μM biotinylated BSA (biotinylated by Barbara Taskinen approximately with three biotin residues per protein molecule) to reduce the non-specific binding of anti-PSA and BSA molecules. Then, biotinylated protein G molecules were injected on the switchavidin layer of an active flow channel at a concentration of 2 μM for 5 minutes to construct a sensing platform that orients anti-PSA molecules perpendicularly to the sensing surface with regenerable interaction. Lastly, both of the flow cells were passivated once again with a 5-min injection of 2 μM biotinylated BSA and blocked with a 5-min injection of 1 mg mL^{-1} BSA in order to minimize the fouling of anti-PSA and BSA molecules.

The dilution series were injected in serial mode from the highest concentration, 200 nM (~ 100*K_D) to the lowest concentration, 20 pM (~ 0.01*K_D) primarily to resolve kinetics and affinity between the Fc-fragment of anti-PSA and the IgG-binding domains of protein G molecules. Secondary aim was to reach the ligand saturation point i.e. the highest immobilization level possible. The reference K_D value used for the calculations of dilutions was 2 nM (Zauner *et al.* 2016). The association time i.e. injection time was 5 minutes for the 20 – 200 nM dilution range of anti-PSA and 10 minutes for the rest of the dilutions. The dissociation time i.e. post-injection time was 9 minutes.

The selective removal of the interactions between the Fc-fragment of anti-PSA and the IgG-binding domains of protein G molecules (termed as "normal regeneration") was performed between the anti-PSA injections by a single 5.5-min injection of 100 mM glycine (pH 2.7) (Zauner *et al.* 2016). A small fraction of switchavidin desorbed expectedly from the biotinylated surface during the first normal regeneration injection and therefore, an extra-injection of 200 nM anti-PSA and a single "dummy" injection of glycine solution was performed prior to the true dilution series. This resulted in a relatively steady baseline within the statistical variation.

4.1.3 Data analysis and kinetic fitting

The statistical analysis of switchavidin immobilization levels was performed using SPSS Statistics software for Windows, version 23 (IBM Corp., Armonk, N.Y., USA).

The kinetic analysis for the biotinylated protein G – anti-PSA interaction was performed using MP-SPR Navi™ DataViewer software, version 4.2.5 (BioNavis) and TraceDrawer™ software, version 1.7 (Ridgeview Instruments, Uppsala, Sweden). The angular position of the SPR peak minimum was determined using an algorithm (called Weighted Centroid) that weights the angular data points near the peak minimum with the corresponding intensity values (Johansen *et al.* 2000). This algorithm takes the non-symmetrical shape of the SPR peak minimum into account, provides a high signal-to-noise ratio of the SPR signal, and is also less sensitive to air bubble-induced noise.

The data processing steps of sensorgram data are illustrated in Figure 7 with schematic pictures. The signals coming from the active and reference flow channel were firstly auto-offsetted regarding the y-axis (intensity) to set a joint baseline level. This facilitated the second step, where the x-axis (time) was offsetted to correct the delay time between the flow cells. In the third step, the SPR signals coming from the active biotinylated protein G coated flow channel were referenced against the biotinylated BSA passivated flow channels.

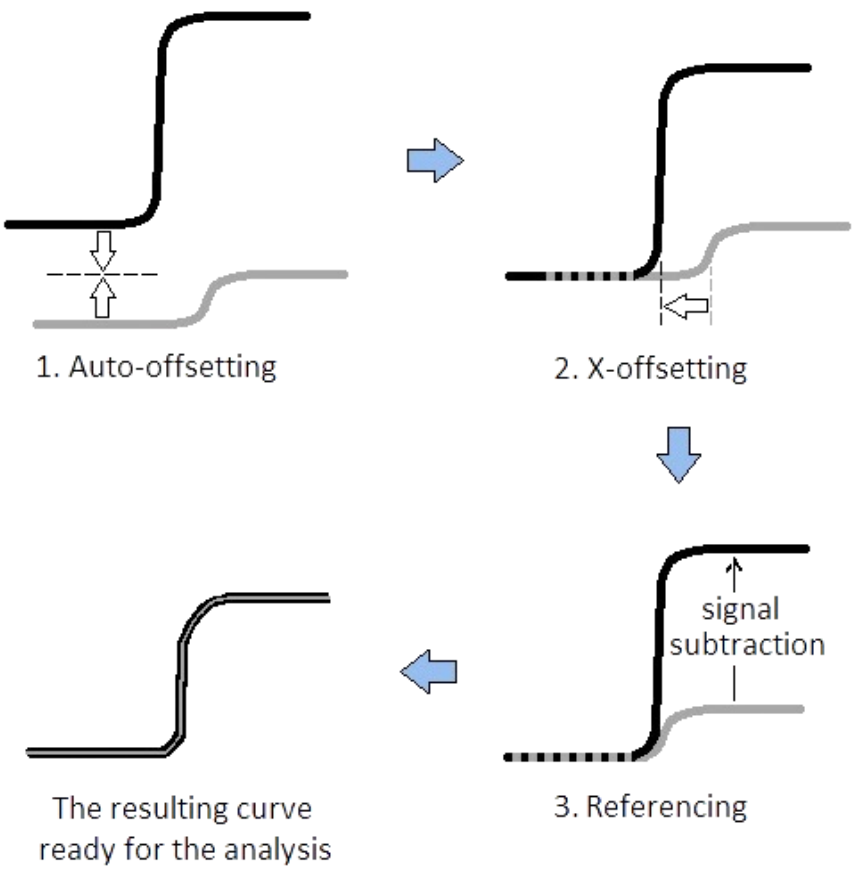

Figure 7. The data processing of sensorgram data. In the first step, the kinetic curves recorded from the active and reference flow channel were auto-offsetted regarding the y-axis (intensity) to make it easier to correct the dead volumes between the flow channels in the second step. The referencing of sensorgram data was performed in the third step, where the signal coming from the reference flow channel was subtracted from the signal coming from the active channel.

In the third step, the starting and ending points of the anti-PSA injections were defined based on the visible association and dissociation phases in respect to the programmed length of the anti-PSA injections. The length of the baseline was set to 5 minutes and the tail parts were set as long as possible.

The advanced kinetic analysis was started by exporting the kinetic curves to TraceDrawer™ software, version 1.7 (Ridgeview Instruments), and typing the accurate anti-PSA concentrations for the individual curves, which were calculated from the concentration of stock solution. The signal spikes originating from the numerous reasons rationalized in section 2.2 were cut from the curves to improve the kinetic fitting. The plotted kinetic data was scaled from angular degrees to millidegrees (mDeg) in order to improve the calculation of kinetic values.

Finally, the kinetic data was fitted to Langmuir and bivalent adsorption models, which correspondingly describe 1:1 and 1:2 binding stoichiometries. The Langmuir fitting is

commonly presented beside bivalent fitting for comparability of kinetic values, but the observed binding rates are empirical and do not reflect the mechanical binding model. The bulk signal was set to zero, and all the other variables were set as global i.e. to be calculated similarly for all the curves. The resulting kinetic and affinity values with the errors, Chi^2, and fitting residuals were reported.

4.2 Interaction kinetics of sulfonamide hCAII inhibitors

4.2.1 Materials

The PBS buffer containing 10 mM phosphate (pH 7.4 at +25 ºC), 137 mM sodium chloride, and 3.7 mM potassium chloride, was prepared by dissolving a single PBS tablet (Sigma-Aldrich) in 200 mL of deionized water.

The standard MP-SPR Navi™ gold sensor slides (as described in section 4.1.1 above) with a 500-nm thick three-dimensional low-density carboxymethylated dextran coating (type CMD 500L) were purchased from XanTec (Düsseldorf, Germany).

The stock solution of a human carbonic anhydrase II (hCAII) enzyme, which was received as a donation from the Tissue Biology research group of professor Seppo Parkkila (Faculty of Medicine and Life Sciences, the University of Tampere), contained 0.1 M Tris-SO_4, 0.4 M NaN_3, 1 mM benzamidine, and 20 % glycerol. According to the amine coupling kit instructions of Thermo Fisher Scientific, all the previously listed additives interfere with the non-specific EDC/NHS amine coupling chemistry. The interfering additives were removed from the protein aliquots by a five-fold ultrafiltration through a Vivaspin® 500 10,000 MWCO PES membrane equipped ultrafiltration device (Sartorius AG, Göttingen, Germany) roughly as described in the user manual of the manufacturer. The MWCO is an abbreviation for the molecular weight cutoff, and it designates the lowest limit for the size of molecule that can be retained in the sample solution during the washing steps. A one size smaller MWCO of PES membrane than recommended for 29 kDa proteins was chosen based on the experience obtained in previous projects (Jenni Leppiniemi, Ph.D., personal communication). This ensures better recovery of the hCAII enzyme.

The immobilization solution of hCAII was prepared in a 10 mM MES buffer, pH 5.70 (2-(N-morpholino)ethanesulfonic acid; Sigma-Aldrich) at a concentration of 0.25 mg mL^{-1}.

The suitable pH for the immobilization solution of the human CAII was estimated to be 0.5 - 1 pH units below the theoretical isoelectric point of the hCAII (pI = 6.86) based on the standard operation procedure commonly used for the EDC/NHS amine coupling chemistry (Fischer 2010). The theoretical isoelectric point of the hCAII was calculated at 280 nm in water using a ProtParam tool (Gasteiger *et al.* 2005) with Swiss-Prot/TrEMBL accession number P00918 (PDB ID: 3HS4. Sippel *et al.* 2009). EDC (MW = 191.70 g mol^{-1}) and NHS (MW = 115.09 g mol^{-1}) reagents were purchased from Sigma-Aldrich. The selected pH of the immobilization solution was validated in further studies based on the steepness and the curvature of the pre-concentration injection responses. In the pre-concentration testing, the enzyme is absorbed into the CMD hydrogel matrix via electrostatic attraction at different pH conditions, which creates varying local enzyme concentrations (https://www.sprpages.nl/immobilization/ligand-pre-concentration; August 22, 2017). The equilibration of the hydrogel matrix and the blocking of the unreacted NHS-ester groups were performed using 0.1 M Na-borate buffer (pH 9.0) with 1 M NaCl, and 1 M ethanolamine (pH 8.5), respectively. These reagents were purchased from Xantec.

Three sulfonamide-based inhibitors of hCAII (acetazolamide, AZE; methanesulfonamide, MSU; 4-sulfamoylbenzoic acid, 4-CBS) were purchased from Sigma-Aldrich for the experiments, in which the interaction kinetics of hCAII with the inhibitors was resolved. The stock solutions of MSU, AZE, and 4-CBS were prepared in PBS buffer containing DMSO (Sigma-Aldrich) solvent or alternatively in pure DMSO. The 20-mM stock solution of the smallest inhibitor, MSU (MW = 95.12 g mol^{-1}), was prepared directly in 3 % (v/v) DMSO solvent containing PBS buffer based on the knowledge of a supervisor. The complete dissolution of larger, AZE (MW = 222.25 g mol^{-1}) and 4-CBS (MW = 201.20 g mol^{-1}), inhibitors required the use of pure DMSO as an intermediate step. In all cases, a slightly smaller quantity than needed for 20 mM inhibitor solution was weighed. Then, the corresponding volume of PBS with 3 % DMSO (density ≈ 1.00 g mL^{-1}) or pure DMSO (density = 1.10 g mL^{-1}) was added accurately with the aid of an analytical balance (Sauter analytical balance, type RE 1612, reproducibility 1 mg; Sauter, Balingen, Germany). The weighed volumes enabled the accurate calculation of inhibitor concentration for the stock solutions. Then, the corresponding 0.1*K_D – 10*K_D dilution series were prepared using PBS without or with 3 % (v/v) DMSO (Davidoff *et al.* 2015). For example, the concentration range of AZE, which extended from 3 nM to 200 nM was prepared by serial two-fold dilutions of the inhibitor stock

solution. A careful preparation of the dilutions series concerning the buffer mismatch has great importance as this may cause problematic bulk effects in the SPR signal.

4.2.2 SPR experiments

The interaction kinetics of hCAII with the inhibitors were measured using the prototype of 420A ILVES MP-SPR Navi™ instrument (BioNavis) equipped with a standard PDMS flow cell that forms four fluidic channels over the sensor surface. The injectables were loaded into the fluidic system of the instrument from a 96-well plate with autosampler-controlled air-bubble segmentation that ensures accurate concentration of sample molecules. The SPR data was recorded with a single wavelength (670 nm) from two enzyme-activated (FC2 and FC4) and two reference channels (FC1 and FC3).

The flow cell temperature was stabilized at an experiment temperature of +25 ºC. The running buffer, protein solutions, and reagents were stabilized at RT and degassed by tapping the liquid filled plastic syringe under negative pressure. The hydrogel matrix of CMD 500L sensor slides was rehydrated and stabilized at the experiment flow rate prior to use until the SPR signal drift was minimal, and a stable baseline was achieved. All the experiments were performed using a flow rate of 20 µL min^{-1} with the exception of the gas removal from the fluidic system, which was performed using a 200 µL min^{-1} flow rate.

Immobilization of hCAII into 3D hydrogel matrix

The hCAII enzyme was immobilized into the hydrogel matrix of a CMD 500L sensor slide using the EDC/NHS amine coupling chemistry. The immobilization was performed in PBS buffer by following the protocol described in the article of Papalia and colleagues in 2006 with minor modifications. At first, the hydrogel matrix was equilibrated for 7 minutes with a 1 M NaCl, 0.1 M sodium borate buffer (pH 9.0) injection that balances the electrostatic interactions of the matrix. Secondly, the carboxyl groups of the hydrogel matrix were activated with a 7-minute injection of freshly prepared 0.4 M (76.7 mg mL^{-1}) EDC / 0.1 M (11.5 mg mL^{-1}) NHS mixture in deionized water that was degassed carefully right before the immobilization solution was loaded into the sample loop. After a 10-minute rinsing step, the immobilization solution of hCAII was introduced on the surfaces of the active flow channels (FC2 and FC4) for 10 minutes. At the end, the unreacted NHS ester groups were blocked simultaneously from all the hydrogel matrices of the flow channels (FC1 – FC4) by a 10-minute injection of

1 M ethanolamine (pH 8.5). The alkalinity of the blocking solution removed also the physisorbed hCAII from the hydrogel matrix.

Interaction kinetics of hCAII with inhibitors

The interaction kinetics of hCAII with the inhibitors was measured at +25 ºC with the highest data collection frequency. PBS with 3% DMSO was used as an immobilization buffer. At the beginning of the dilution series, two blank injections of the running buffer were added to test the stability of the enzyme-immobilized matrices. Then the inhibitor dilutions were injected in serial mode for 4.5 minutes from the lowest to the highest concentration with a 6-minute delay time (dissociation phase) between the injections.

4.2.3 Data analysis and kinetic fitting

The kinetic analysis for the interactions between hCAII and sulfonamide inhibitors was performed using MP-SPR Navi™ DataViewer (BioNavis) and TraceDrawer™ (version 1.8; Ridgeview Instruments). The SPR data was recorded from two active (FC2 and FC4) and two reference channels (FC1 and FC3). The angular position of SPR peak minimum was determined using the Weighted Centroid algorithm (Johansen *et al.* 2000). This increases the signal-to-noise ratio, which is beneficial especially in small MW analyte detection.

The data processing steps of sensorgram data were illustrated earlier in Figure 7 in section 4.1.3 with schematic pictures. Firstly, the SPR peak minimum signals coming from the active and reference flow channel were auto-offsetted to a joint baseline level. This facilitated the second step, where the x-axis (time) was offsetted to correct the dead volumes between the flow cells. In the third step, the SPR signals coming from the active hCAII enzyme-immobilized flow channels (FC2 and FC3) were referenced against the non-modified flow channels (FC3 and FC4), respectively.

The start and end points of the inhibitor injections were defined based on the visible association and dissociation phases in respect of the programmed lengths of the inhibitor injections. The length of the baseline was set as constant and the tail part was set as long as possible.

The advanced kinetic analysis was started by exporting the kinetic curves to TraceDrawer™ software and entering the accurate inhibitor concentrations for the individual curves, which were calculated from the concentration of the stock solution. The signal spikes were cut from

the curves to improve the kinetic fitting. The plotted kinetic data was scaled from degrees to mDeg in order to improve the calculation of kinetic values.

The dissociation rate constant was determined and set as constant before the kinetic data was fitted globally in a Langmuir adsorption model, which describes 1:1 binding stoichiometry where one inhibitor molecule binds one enzyme molecule at a time. The bulk signal was set to zero. The resulting kinetic and affinity values with the errors, Chi^2, and fitting residuals were reported.

5 RESULTS

5.1 Immunosensing platform with stepwise regeneration

The SPR signal measured at 785 nm laser wavelength showed low combined drift for the instrument and the b-SAM surface. The immobilization levels of switchavidin were repeatable and reproducible, the switchavidin layer pointed out clear ultra-low fouling ability against common model proteins, and the two-step regeneration of the sensing platform shows practical resolution between two regeneration solution compositions. Furthermore, some observations concerning MP-SPR detection of the multivalent binding mechanism of switchavidin to b-SAM surface are presented. Based on the results presented in this chapter, the tentative diagnostic performance of the sensing platform is determined later in the discussion chapter.

5.1.1 Stability of the instrument and b-SAM

To assess the combined stability of the instrument and b-SAM on a gold sensor slide, the baseline drift of the SPR peak minimum angle was analyzed for a 30-minute time period at stabilized temperature and buffer flow conditions. The results listed in Table 1 were obtained from two parallel flow cells of three randomly chosen sensors. The baseline drift was reported at two wavelengths in mDeg min^{-1} with corresponding sample standard deviations.

Table 1. Baseline drift of SPR peak minimum angle. The drift values were measured for three sensors in mDeg min^{-1} at two laser wavelengths (670 nm and 785 nm). Flow channel and laser wavelength –specific means and sample standard deviation (SD) were reported.

		Baseline drift (mDeg min^{-1})				
	Wavelength (nm)	**Sensor #1**	**Sensor #2**	**Sensor #3**	**Mean[a]**	**SD[a]**
Upper FC[b]	670	+0.22	+0.06	+0.14	+0.14	±0.08
	785	+0.20	+0.05	+0.11	+0.12	±0.08
Lower FC[b]	670	+0.42	+0.08	+0.18	+0.23	±0.17
	785	+0.32	+0.06	+0.11	+0.16	±0.14

[a] Calculated in mDeg min^{-1}

[b] FC is an abbreviation for the “flow channel”

The calculated values for the baseline drift were smaller for the upper flow channel than for the lower flow channel at both wavelengths. The direction of the baseline drift was upwards in all cases. The sample standard deviations were smaller for the upper flow channel than for the lower flow channel.

5.1.2 Immobilization levels of switchavidin

The immobilization solution of switchavidin was assessed free from nucleic acid contaminants based on the 260/280 nm absorbance ratios, which were close to 0.57 (Raynal *et al.* 2014). The switchavidin immobilization levels on the b-SAM were analyzed from eight sensor slides with at least two repeats per each sensor (N = 25) (shown in Figure 8). The values presented in the graphs are reported only at laser wavelength 785 nm for directional comparability to values measured in the reference article at laser wavelength 760 nm of the Biacore® instruments.

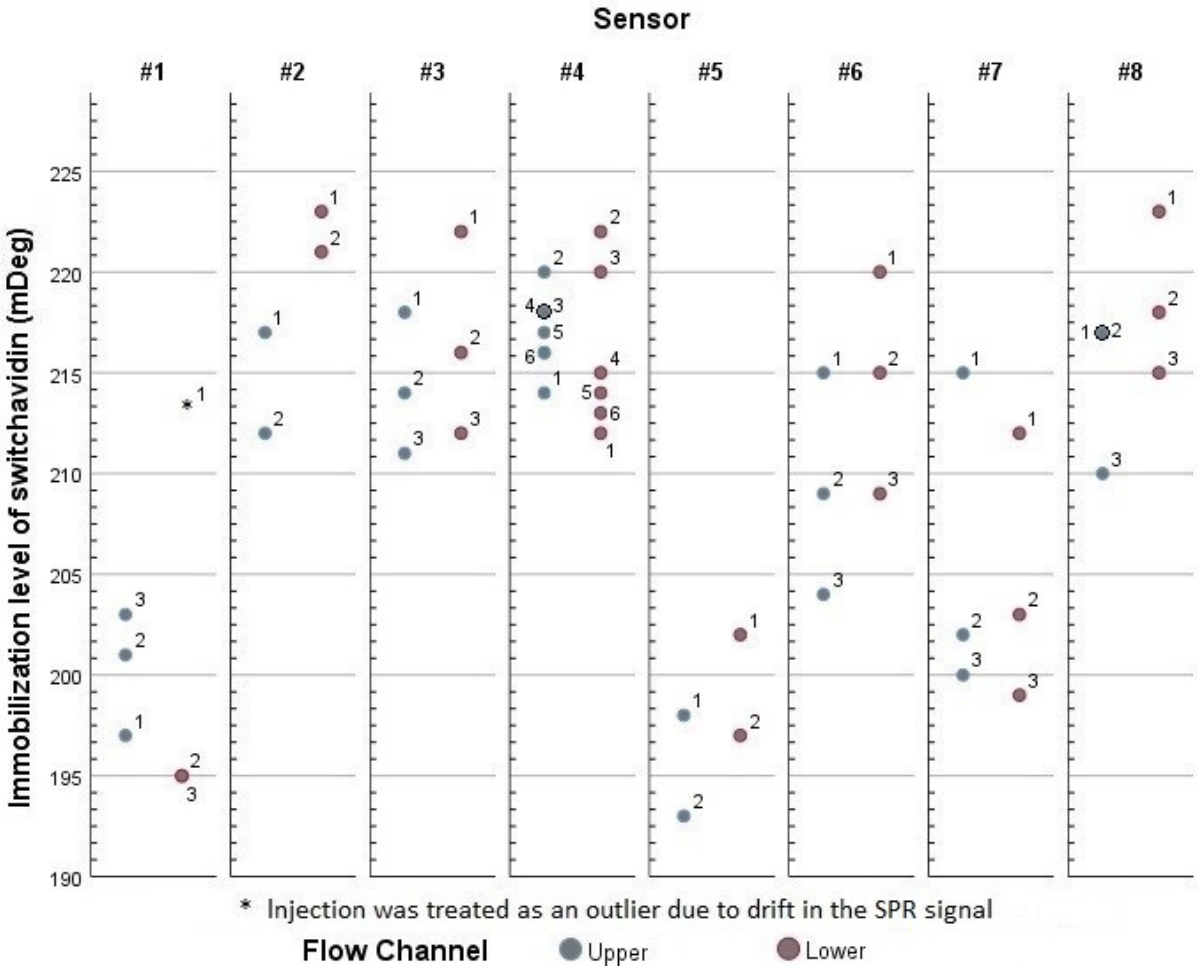

Figure 8. Sensor-specific immobilization levels of switchavidin in mDeg. The upper and lower channel of the flow cell are denoted with grey and red circles, respectively. The cycle numbers are shown together with the data points. First switchavidin injection to the lower flow channel of the sensor #1 was excluded from the dataset due to drift in the SPR signal.

The variables were qualified as approximately normally distributed based on the skewness values calculated by SPSS software. A small number of repeats, however, justified only the use of non-parametric tests in the statistical analysis. The arithmetic mean of switchavidin immobilization levels calculated from the sensor-specific averages for the upper and lower flow channels were 210.2 (SD 7.9) mDeg and 212.2 (SD 8.9) mDeg, respectively. The sample standard deviations correspond to less than 4.5 % variation in the immobilization levels. Independent-Samples Kruskal-Wallis test showed statistical difference between different sensors ($p = 0.022 < 0.050$). The comparison of flow cell-specific values by Wilcoxon test instead did not show a statistically significant difference between the flow cells ($p = 0.093 > 0.050$).

The scatter plot of sensor-grouped switchavidin immobilization levels presented in Figure 9 shows a decreasing trend between the cycles. Switchavidin injections affected by regeneration-solution-induced drift were treated as outliers in the statistical analysis. Notably, the statistical analysis of switchavidin immobilization levels between the two flow cells was found to be sensitive to the existence of outliers in the analyzed dataset. When a single outlier was left in the dataset, the straightforwardly used paired T-test resulted in p-value of 0.049, which technically indicates statistically significant difference ($p < 0.050$) between the flow cell-specified immobilization levels. The exclusion of the concerned outlier resulted in p-value of 0.093 so there was no statistically significant relationship ($p > 0.050$) between the variables under the restrictions of the dataset.

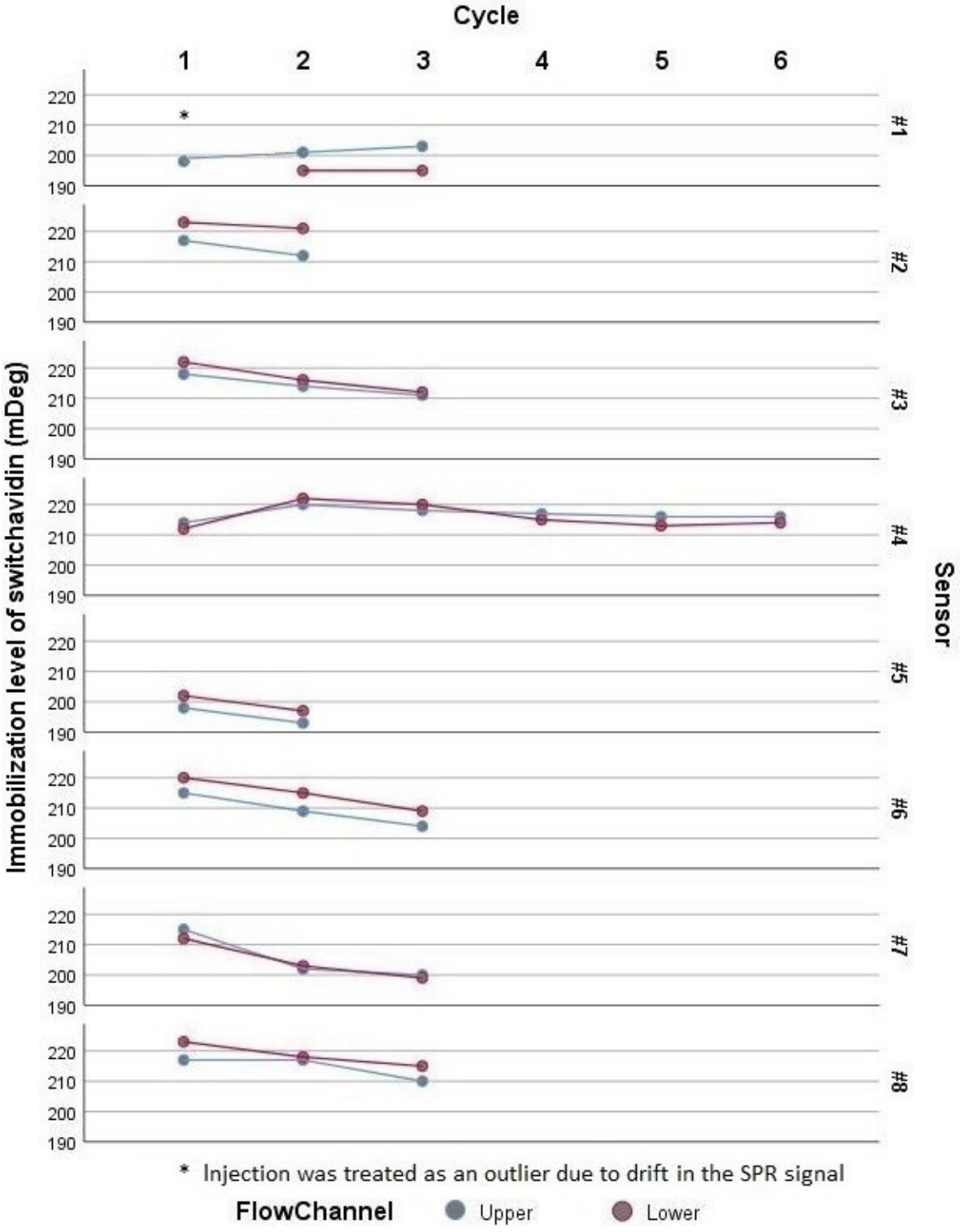

Figure 9. Immobilization levels of switchavidin at different cycles in mDeg. Sensor-specific values are presented in separate rows. The immobilization levels of the upper and lower flow channel are marked with grey and red circles, respectively. First switchavidin injection to the lower flow channel of the sensor #1 was excluded from the dataset due to drift in the SPR signal.

5.1.3 Mechanical binding model of switchavidin molecules

The adsorption of (strept)avidin molecules on the planar biotinylated surfaces involves specific binding mostly via one or two biotin-(strept)avidin bridges as well as non-specific interactions among adsorbing proteins (cohesion) or between protein and immobilization surface (adhesion) (Dubacheva *et al.* 2017). These simultaneously occurring processes are, however, extremely difficult to model and verify. This section presents transient peaks, logarithmic decreases, and elevations observed in PMI signal, which support the later discussion of the mechanical adsorption model proposed of switchavidin on the b-SAM membrane.

A transient peak and following logarithmic decrease and elevation in PMI data after the beginning of switchavidin adsorption were monitored in order to track changes in protein orientation or conformation leading to fluctuations in the surface area per molecule. Figure 10 presents corresponding data from a single sensor slide for three experiment cycles.

The transient peak seen in the first experiment cycle was higher than the subsequent peaks of the second and third experiment cycle. The elevation of the first cycle seemed to come earlier than the elevations seen for the second and third cycle.

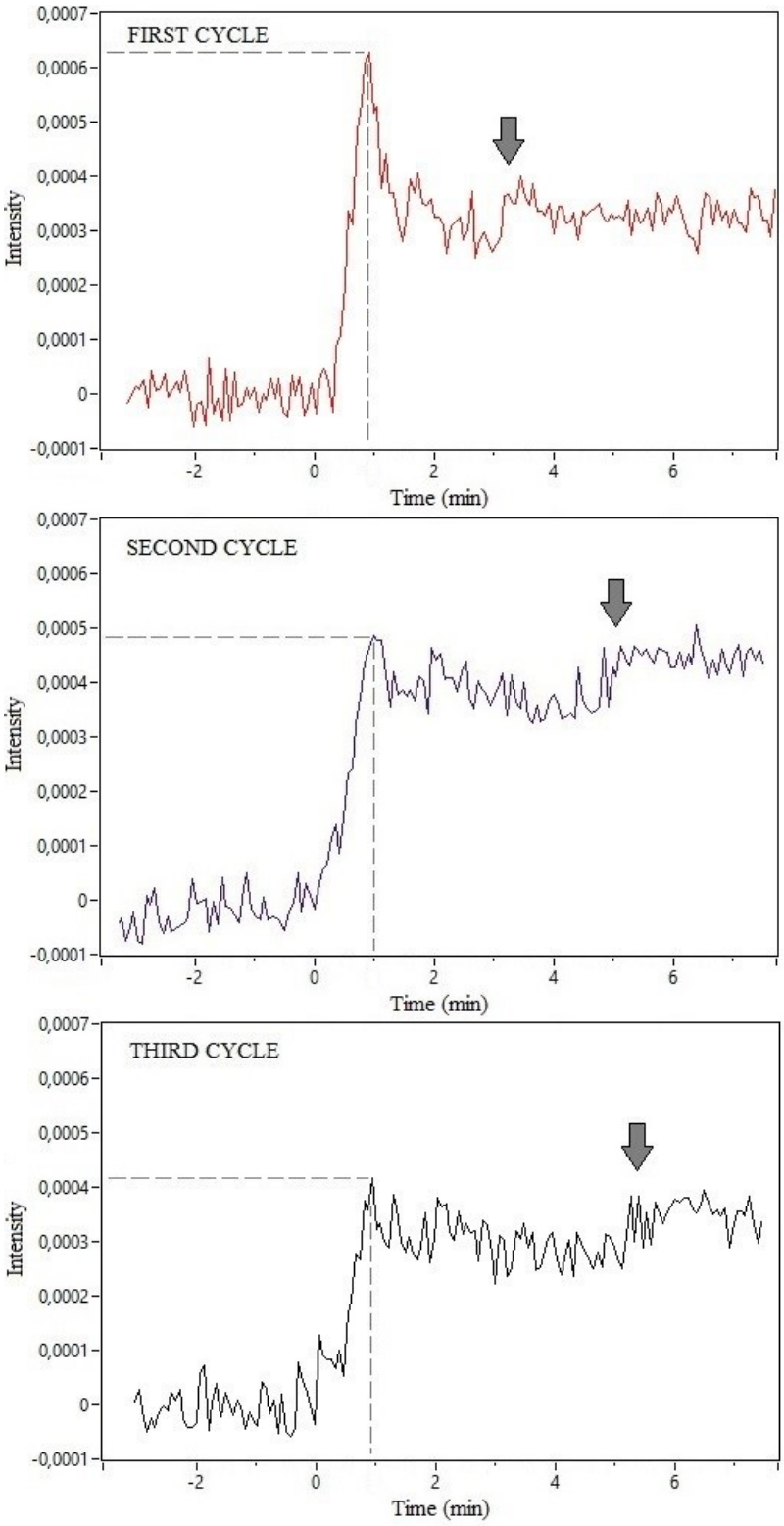

Figure 10. A compilation picture of transient peaks and elevations observed in the SPR peak minimum intensity (PMI) signal from three cycles of switchavidin adsorption. The adsorption of switchavidin starts from zero minutes. The amplitudes and the time points of transient peaks are pointed with grey dashed lines. The grey arrows denote the positions of signal elevations.

5.1.4 Regeneration of immunosensing platform

The first two baseline shifts after the first normal regeneration cycle (i.e. “dummy” injection) were roughly -5 mDeg, which corresponds to 2.4 % of mean adsorbed switchavidin (~211 mDeg), but later the baseline shift settled to -2 mDeg (0.9 %). Unfortunately, there was only a single sensor slide available for analyzing these baseline shifts.

The baseline shifts after the first rigorous regeneration of the switchavidin layer by the combination of citric acid and SDS resulted in varying amounts of residual switchavidin or slight deterioration of the b-SAM. Later rigorous regeneration cycles showed more stable baseline shift, which was +3.7 mDeg for the upper flow channel, and corresponds to 1.8 % of mean adsorbed switchavidin (~211 mDeg). Related measurement data shown in Figure 11 was collected from various experiments with different protein compositions on top of the switchavidin layer, which means that obtained values for the baseline shift are unqualified to predict statistical behavior. However, a tentative analysis of trends can be deduced within a sensor.

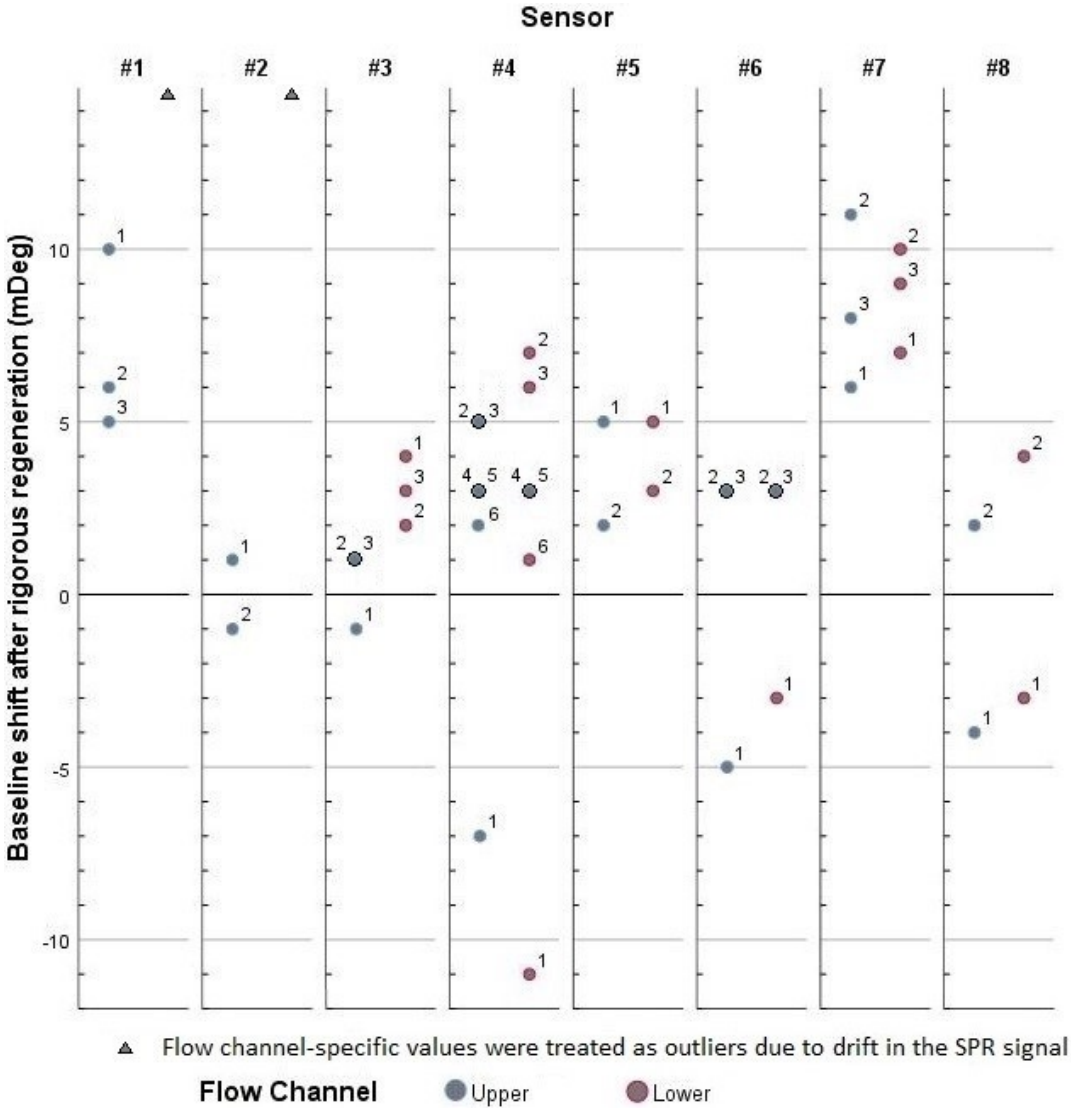

Figure 11. The baseline shift after a rigorous regeneration treatment in mDeg. Sensor-specific values are categorized in separate columns. The immobilization levels of the upper and lower flow channel are marked with grey and red circles, respectively. The identical values for two cycles were fortified with black circle. The baseline shift values recorded from the lower flow channel of sensor #1 and #2 were removed from the dataset due to drift in the SPR signal.

Relative regeneration efficiency (shown in Figure 12) was calculated for the rigorous regeneration with eight sensors from the immobilization levels of switchavidin (presented in Figure 8) and corresponding baseline shift values obtained after rigorous regeneration treatment (presented in Figure 11).

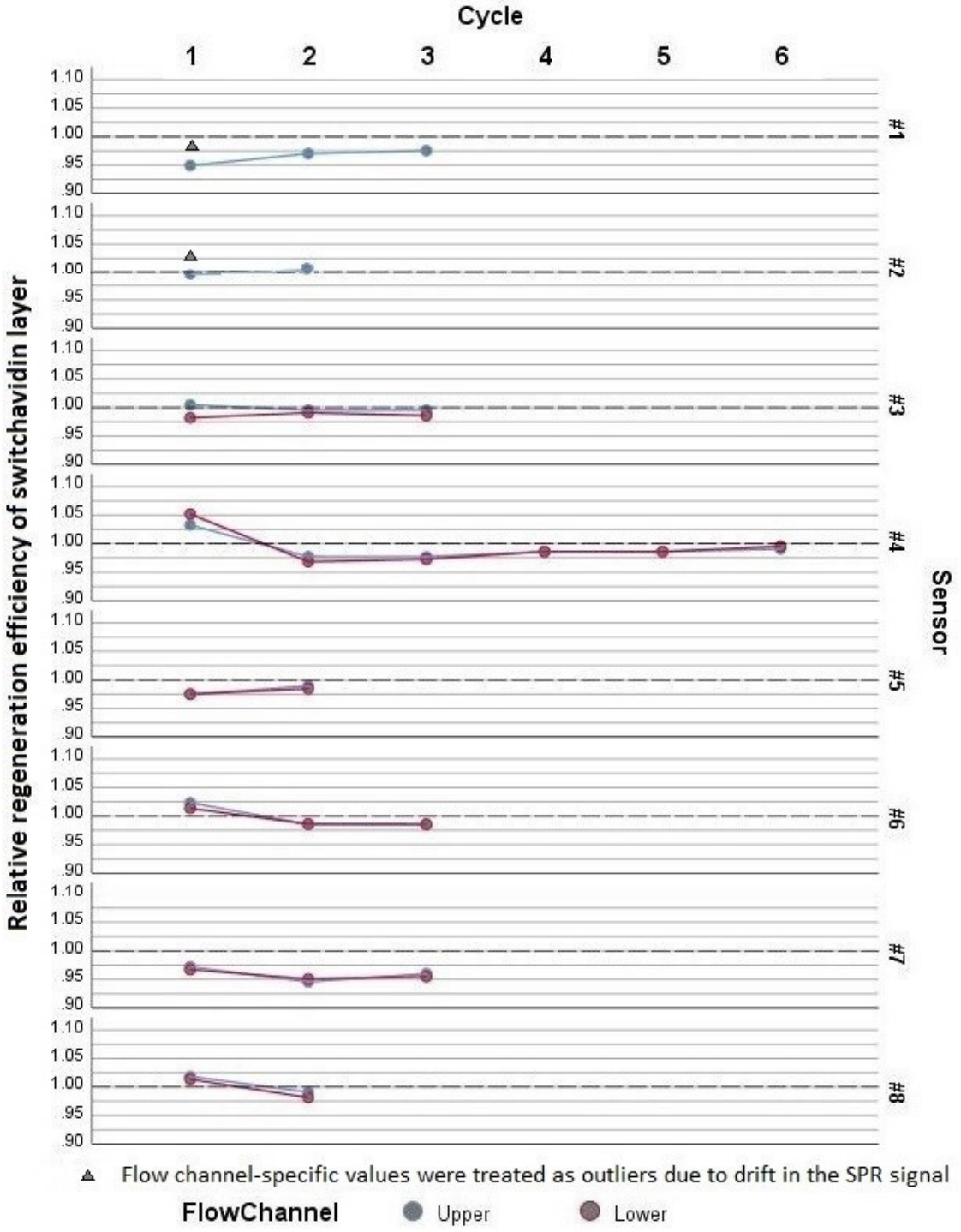

Figure 12. The relative regeneration efficiency of rigorous regeneration in respect of the cycle. Sensor-specific values are presented in separate rows. The upper and lower flow channel are marked with grey and red circles, respectively. The relative regeneration efficiency values of the sensor #1 and #2 were removed from the data set due to drift in the SPR signal.

Ratio 1.00 means that the regeneration process is capable to remove no more than previously adsorbed switchavidin and subsequent mediators from the b-SAM. Ratios lower than 1.00

imply roughly that the regeneration injection is unable to remove all switchavidin (and bridged or stably crosslinked proteins on top of the switchavidin layer) from the biotinylated SAM surface. Ratios higher than 1.00 instead suggest that the regeneration treatment removes more than only the switchavidin molecules from the gold surface.

5.1.5 Anti-fouling ability of switchavidin layer

The anti-fouling ability of the switchavidin layer was assessed by injecting the single protein solutions of BSA, lysozyme, and h-IgG over the switchavidin surface, and comparing the SPR signal amplitudes (shown in Table 2) to general standards. Furthermore, the completeness and efficiency of BSA blocking was tested by blocking one flow channel twice with BSA before lysozyme or h-IgG injections, and comparing the signal amplitudes of BSA injections together as well as with the signal amplitudes obtained from the non-blocked flow channel in overall. The immobilization solutions of concerned proteins were assessed free from non-protein contaminants prior to the experiments based on the 260/280 nm absorbance ratios that were close to 0.57 (Raynal *et al.* 2014). The mean fouling levels for BSA and lysozyme were obtained from two sensors with six repeats and they were reported in mDeg with corresponding sample standard deviations.

The highest mean fouling amplitude (0.6 mDeg) was observed for the first injection of lysozyme on the non-blocked switchavidin surface. This corresponds roughly to 6 pg mm^{-2} or 0.3 % percent adsorption on the average switchavidin monolayer (~ 211 mDeg). The second BSA injection (2nd BSA) gave the same signal response within the sensor as the first BSA injection (1st BSA) on the intact switchavidin layer.

Table 2. The fouling levels of the switchavidin layer against BSA and lysozyme on BSA-blocked and non-modified surface in mDeg. Arithmetic mean and sample standard deviation (SD) were calculated for the fouling levels at the different stages of the adsorption layer. Asterisk (*) denoted values were excluded from the data set due to drift in the SPR signal.

	Fouling level (mDeg)							
Sensor	**#1**		**#2**					
Cycle	**1**	**2**	**1**	**2**	**3**	**4**	Mean (mDeg)	SD (mDeg)
1st BSA	1.7	0.0	0.0	*	0.5	0.2	0.5	0.7
2nd BSA	1.7	0.0	0.0	0.5	0.5	*	0.5	0.7
1st Lysozyme (BSA blocked)	0.5	0.2	1.0	0.8	*	0.0	0.5	0.4
2nd Lysozyme (BSA blocked)	0.5	0.2	0.0	-1.1	*	0.2	0.0	0.6
1st Lysozyme (non-blocked)	0.5	0.0	1.0	0.4	1.2	0.5	0.6	0.4
2nd Lysozyme (non-blocked)	0.0	0.0	0.2	-0.3	0.3	-0.3	0.0	0.2

The mean fouling levels of lysozyme on the BSA-blocked surface were 0.5 mDeg after the first lysozyme injection and 0.0 mDeg after the second lysozyme injection. The mean fouling levels of lysozyme on the non-blocked surface were 0.6 mDeg after the first lysozyme injection and 0.0 mDeg after the second lysozyme injection.

The mean fouling levels for BSA and h-IgG (presented in Table 3) were obtained from two sensors with four repeats and they were reported in mDeg with corresponding sample standard deviations.

The highest mean fouling amplitude (3.0 mDeg) was observed for the h-IgG injection on the non-blocked switchavidin surface. This corresponds roughly to 30 pg mm^{-2} or 1.4 % percent adsorption on the average switchavidin monolayer (~ 211 mDeg). The response of the second BSA injection (2nd BSA) after the first BSA blocking (1st BSA) of the intact switchavidin layer was ambiguous. The mean fouling levels of h-IgG on the BSA blocked and non-blocked surfaces were 1.4 mDeg and 3.0 mDeg, respectively.

Table 3. The fouling levels of BSA and h-IgG on BSA-blocked and non-blocked switchavidin layers in mDeg. Arithmetic mean and sample standard deviation (SD) were calculated for the fouling levels at the different stages of the adsorption layer. Asterisk (*) denoted values were excluded from the data set due to drift in the SPR signal.

	Fouling level (mDeg)					
Sensor	**#1**	**#2**				
Cycle	**1**	**1**	**2**	**3**	Mean (mDeg)	SD (mDeg)
1st BSA	1.5	0.7	1.8	-0.3	0.9	0.9
2nd BSA	2.4	-0.7	0.0	1.3	0.8	1.4
h-IgG (BSA blocked)	-3.3	6.0	*	*	1.4	6.6
h-IgG (non-blocked)	1.0	5.0	*	*	3.0	2.8

5.1.6 Kinetics of biotinylated protein G – anti-PSA interaction

The reference flow channel was passivated with biotinylated BSA, the active flow channel was activated with biotinylated protein G, and the binding kinetics between the Fc fragment of the anti-PSA molecule and the IgG-binding domains of the biotinylated protein G molecules was measured by injecting an applicable range of anti-PSA dilutions over a freshly constructed sensing surface.

The truthful binding model for the biotinylated protein G – anti-PSA interaction lie somewhere between a simple Langmuir (OneToOne) fitting model and more complex bivalent (TwoToOne) fitting model due to the binding stoichiometry of the Fc fragment, and the heterogeneity in the spacing of the mediator molecules. This ultimately led to the presentation of both Langmuir and bivalent fitting for the interaction curves. Association and dissociation constants as well as affinity, B_{max} and Chi^2 values were reported with corresponding deviations only at wavelength 785 nm.

The immobilization solutions of biotinylated protein G, biotinylated BSA and anti-PSA were confirmed free from nucleic acid contaminants prior to the experiments based on the 260/280 nm absorbance ratios, which were close to 0.57 (Raynal *et al.* 2014).

Applicable measurement data was obtained only from a single anti-PSA dilution series. The immobilization levels of the biotinylated protein G and biotinylated BSA were 44 mDeg and 101 mDeg, respectively. The interaction kinetics measured between biotinylated protein G and anti-PSA was fitted in Langmuir (Figure 13) and bivalent (Figure 14) adsorption models, and the calculated kinetic constants were presented with corresponding standard deviations. The quality of fittings was evaluated further based on the residual plots presented in Figure 15 and Figure 16.

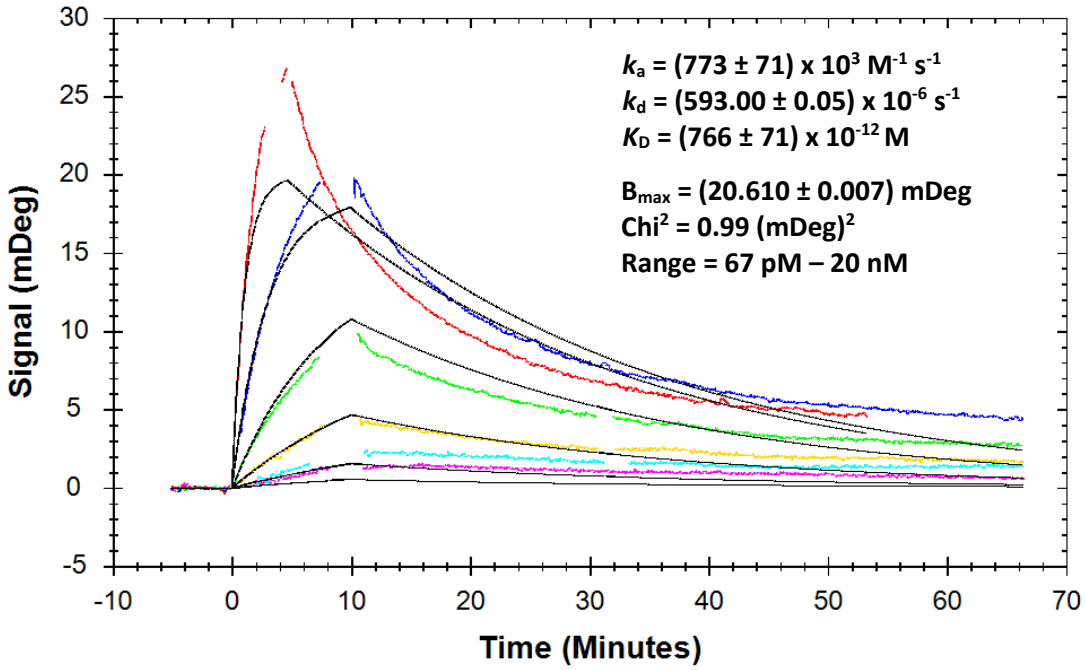

Figure 13. Kinetic curves of the biotinylated protein G – anti-PSA interaction measured for 67 pM – 20 nM concentration range (colored curves) and fitted in a Langmuir model (black curves). Signal levels of adsorption are presented in mDeg. Association and dissociation rate constants (k_a and k_d) as well as the dissociation constant (K_D), maximum signal response that ligands can generate (B_{max}), and Chi^2 values are reported with corresponding deviations.

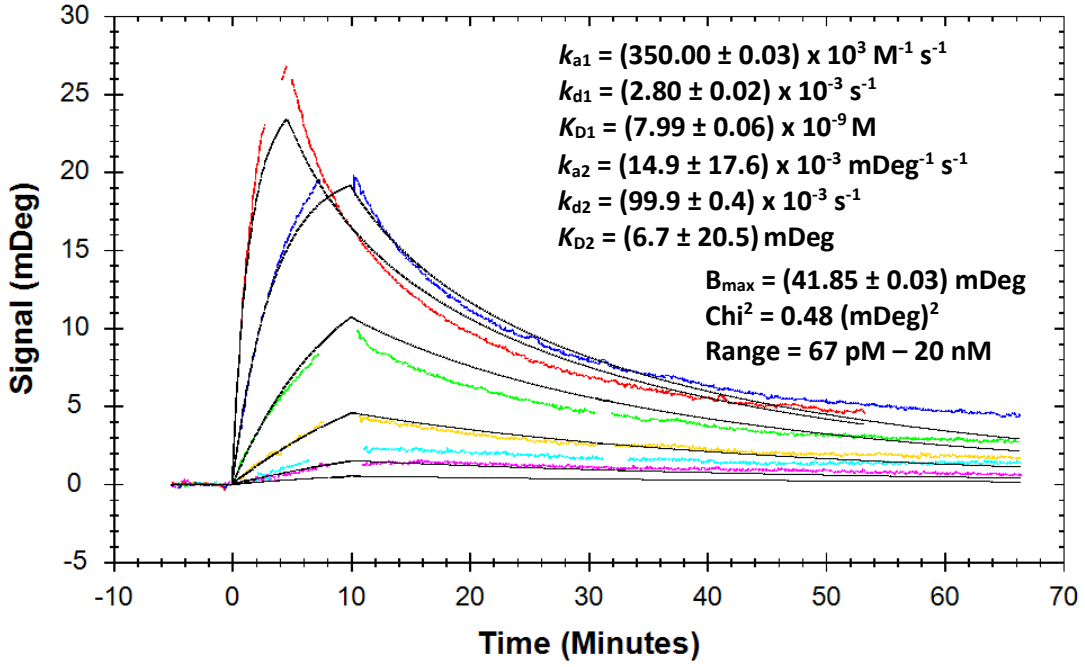

Figure 14. Kinetic curves of the biotinylated protein G – anti-PSA interaction measured for a 67 pM – 20 nM concentration range (colored curves) and fitted in bivalent model (black curves). Signal levels of adsorption are presented in mDeg. Association and dissociation rate constants (k_a and k_d) as well as dissociation constant (K_D), and maximum signal response that ligands can generate (B_{max}) are reported for the monovalent and divalent phase of the interaction with corresponding deviations and Chi^2.

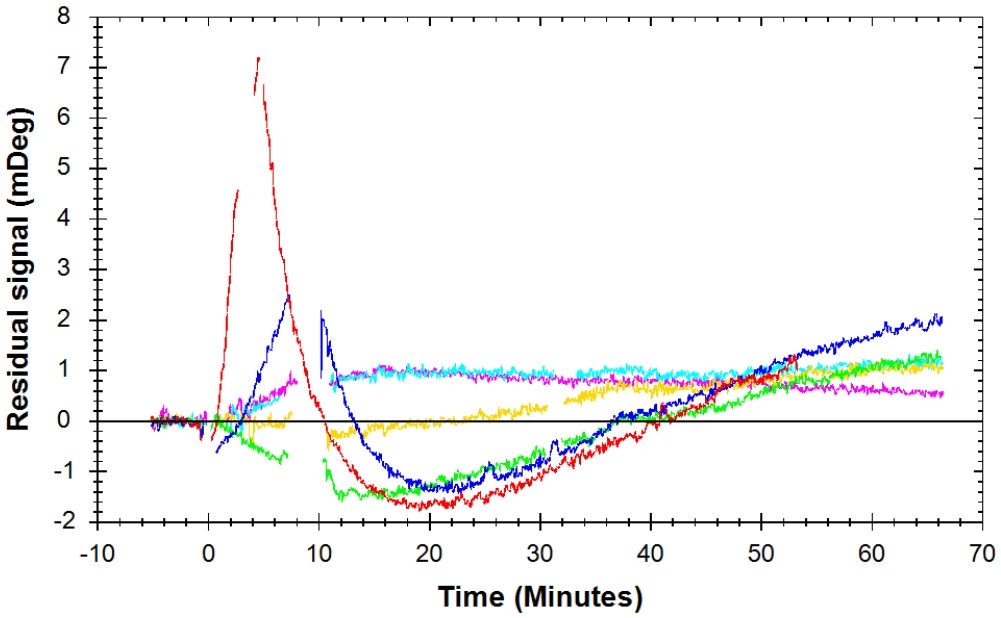

Figure 15. The residual signal of Langmuir fitting performed for the biotinylated protein G – anti-PSA interaction. The residual signal was reported in mDeg with corresponding coloring of concentrations as in Figure 13.

Small systematic differences between the curve fitting and the measured curves were seen for the Langmuir fitting (shown in Figure 13) of the anti-PSA injections having higher concentrations than 1 nM (cyan fitting curve).

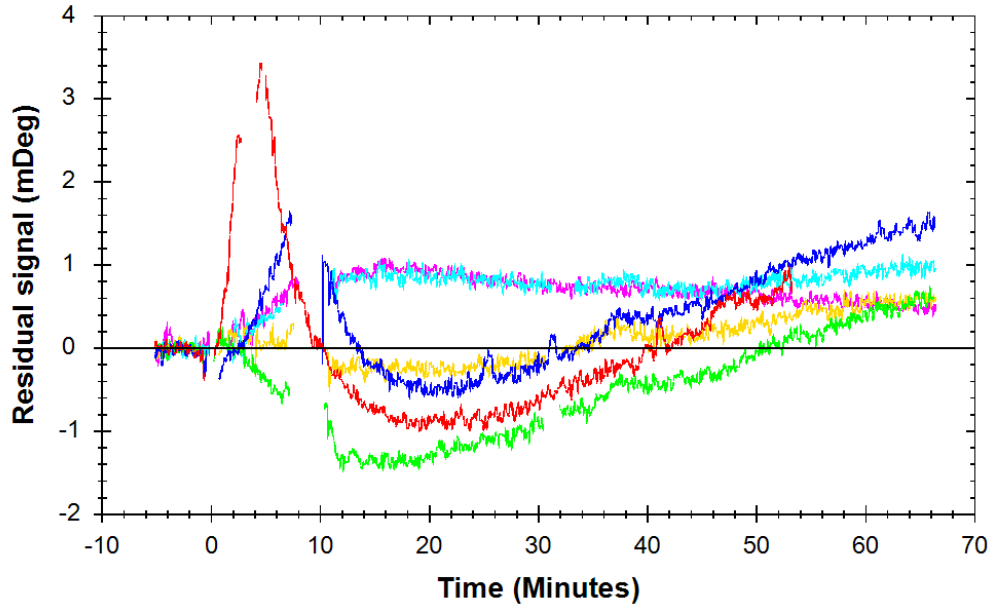

Figure 16. The residual signal of bivalent fitting performed for the biotinylated protein G – anti-PSA interaction. The residual signal was reported in mDeg with corresponding coloring of concentration as in Figure 14.

Similar although smaller differences between the curve fittings and the measured curves were seen for the bivalent fitting (shown in Figure 15) than for the Langmuir fitting (shown in Figure 16) of the anti-PSA injections at higher concentrations than 1 nM (cyan fitting curves).

5.2 Interaction kinetics of sulfonamide hCAII inhibitors

5.2.1 Immobilization of hCAII enzyme

The human CAII enzyme was immobilized into a carboxymethylated dextran matrix using the EDC/NHS amine coupling chemistry in order to measure the interaction kinetics of hCAII with three inhibitors. The immobilization level of hCAII used in the successful inhibitor binding cycle performed with AZE was 675 mDeg. The pH of immobilization buffer was adjusted to 5.70 based on the theoretical isoelectric point of hCAII (pI = 6.86).

5.2.2 Detection of hCAII interaction kinetics with inhibitors

The hCAII interaction kinetics with three inhibitors (4-CBS, AZE, and MSU) were measured from the lowest inhibitor concentration to the highest inhibitor concentration. Unfortunately, the general quality of the kinetic data was poor due to challenges associated with the enzyme immobilization and air bubble management. Fortunately, one applicable dataset was recorded for a single dilution series of AZE from a single sensor. The kinetic curves were fitted to the Langmuir model (presented in Figure 17). The quality of the fitting was evaluated further based on the residual plot shown in Figure 18.

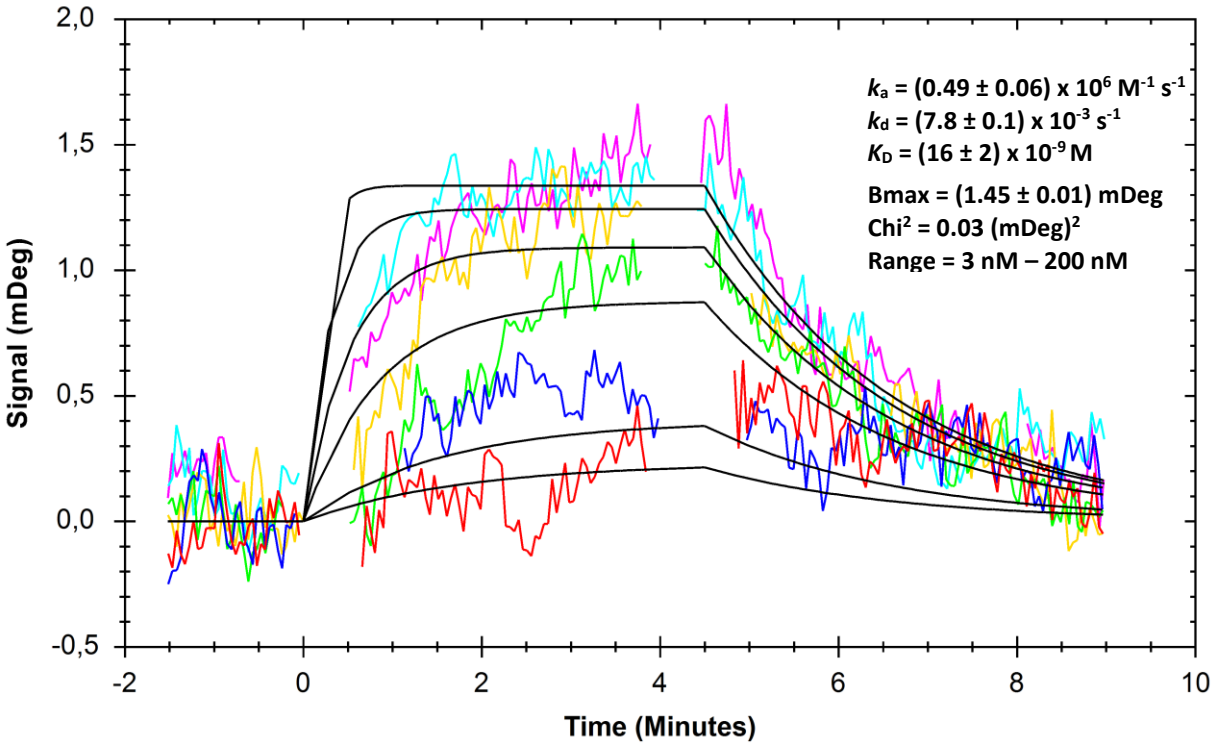

Figure 17. Kinetic curves of the hCAII – AZE interaction measured for a 3 nM – 200 nM concentration range (colored curves without 12.5 nM dilution) and fitted in the Langmuir model (black curves). The cutting of the signal peaks resulted in gaps into the measurement data.

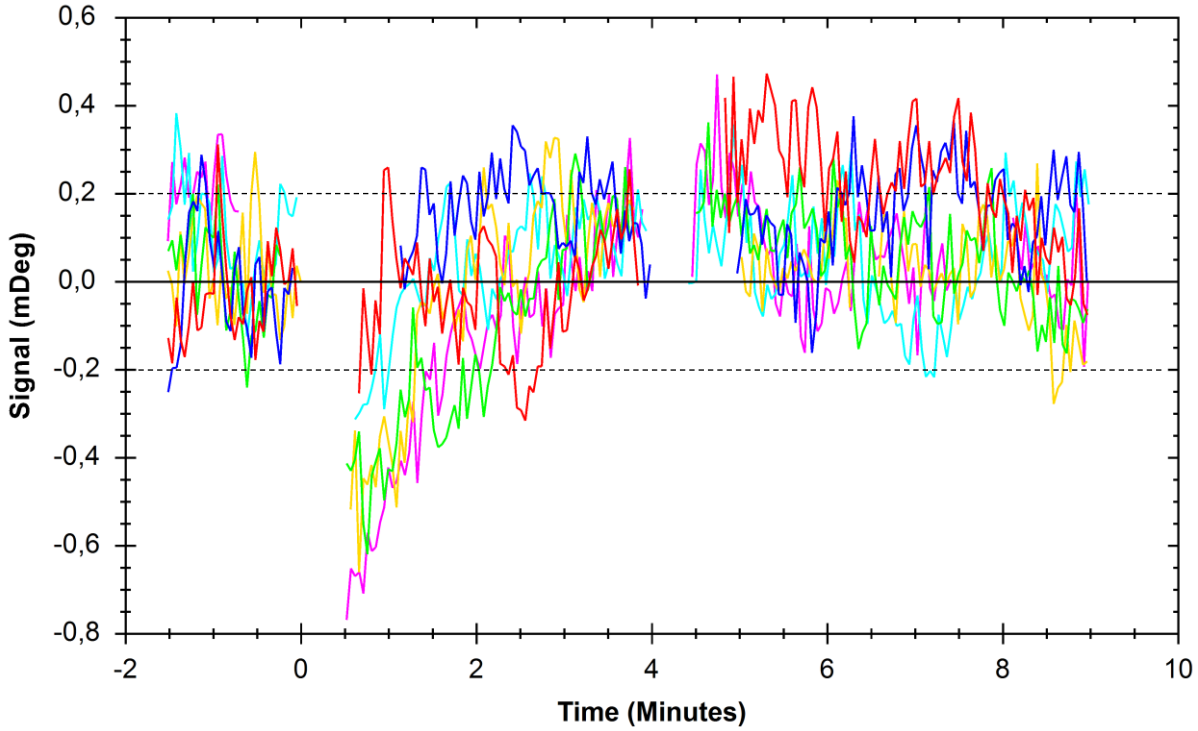

Figure 18. The residual signal of Langmuir fitting performed for the hCAII – acetazolamide interaction data in mDeg. The cutting of the signal peaks resulted in gaps into the measurement data. The noise level of the enzyme-coupled sensing surface is marked with dashed lines.

The kinetic fitting of the hCAII – acetazolamide interaction data into the Langmuir model was successful in terms of calculated fitting residuals, which varied inside the noise level of the measurements (marked with dashed lines in Figure 18), but clear systematic deviations were observed in the beginning of the association and dissociation phases.

6 DISCUSSION

6.1 Immunosensing platform with stepwise regeneration

6.1.1 Stability of instrument and b-SAM

The stability of the instrument and b-SAM was assessed based on the baseline drifts observed in the SPR peak minimum angle measurements. The origin of baseline drift often remains unclear, but it may be attributed to the fluctuations in the flow cell temperature or the contaminants in the fluidic system as well as the buildup of gas onto the sensing surface or the instability of molecules bound on the gold surface (Biacore™ Assay Handbook 2012). The measurements were performed with sterile filtered PBS running buffer at a constant flow rate after thorough cleaning of the instrument and stabilization of experiment conditions. Prior the experiment, the thermal drift was minimized with RT equilibrated running buffer and the flow cell temperature was stabilized with a Peltier-type temperature controller that is capable of adjusting flow cell temperature both upwards and downwards. The buildup of gas onto the b-SAM surface was reduced using RT equilibrated running buffer that was degassed by tapping the buffer filled plastic syringe under negative pressure. The buildup of residual gas was followed by monitoring the PMI signal, and the stability of PMI signal was exploited when a 30-min time period was selected for the baseline drift analysis.

The directional comparison of recorded baseline drifts can be made with the instrumental drift reported on the specifications of the 210A VASA MP-SPR Navi™ instrument. The baseline drifts were measured from three sensor slides. The sensor-specific baseline drift values were higher for the 670-nm wavelength lasers than for the 785-nm wavelength lasers. The mean baseline drifts of the upper and lower flow channel reported at 785 nm-wavelength lasers for comparability with the reference system of Biacore were on average 0.12 mDeg min^{-1} and 0.16 mDeg min^{-1}, respectively. Those values are very close to the reported instrumental drift (> 0.1 mDeg min^{-1}) when the additional b-SAM molecular layer of the studied sensing surface is taken into account.

Small and systematically occurring differences in the sensor-specific baseline drifts between the flow channels could be explained with the inaccuracies in the specified wavelengths of the lasers (Zhang *et al.* 2003). This would lead to the divergent sensitivities of the measurement

spots to the fluctuations in the experiment conditions. It was estimated that the variation between the laser wavelengths could be in the range of ±5 nm (Tony Stoor, BioNavis, personal communication). The dependence of the baseline drift on the wavelengths of lasers could be simply tested in future studies by comparing the flow channel-specific baseline drift results together when the sensor slide is rotated in the sensor holder i.e. the flow channels are transposed. Small, although visible, deviations between the specified wavelength of different flow channels are difficult to eliminate in ultrasensitive sensing systems, but fortunately the relevance of the effects on the immunosensing applications is marginal.

In summary, the carefully performed priming and conditioning with high quality buffer and accurate temperature control of the flow cell resulted in sufficiently low baseline drift for the combination of b-SAM and the instrument in comparison with the instrumental drift. This provides a secure platform for the construction of mediator and ligand layers, but the statistical significance of the results cannot be defined due to the low number of measured sensor slides.

6.1.2 Immobilization levels of switchavidin

The purity as well as integrity and homogeneity are crucial properties for the immobilization solutions of proteins in terms of valid immobilization levels and interaction kinetics. The purity and integrity of the switchavidin protein solutions had been qualified using a SDS-PAGE method and a UV-Vis spectrophotometer, but the purity from non-protein contaminants was reassessed as pure based on the absorbance ratio A280/260 measured by a UV-Vis spectrophotometer (http://biomeditech.fi/Protein_Shop/switchavidin.html; July 1, 2017).

Dynamic light scattering (DLS) would have provided information about the homogeneity of switchavidin solution by measuring the monodispersity based on the size of the particles. The determination of monodispersity for the switchavidin immobilization solution would have ensured that the switchavidin molecules are consistently in a soluble tetrameric state, and that the protein handling or the storage conditions of the protein solution have not formed aggregates. (Raynal *et al.* 2014)

The mean switchavidin immobilization levels for the upper and lower flow channels were 210.2 (SD 7.9) mDeg and 212.2 (SD 8.9) mDeg, respectively. These values were lower than the reference adsorption level (2416 ± 8 RU i.e. response units that roughly corresponds to 241.6 ± 0.8 mDeg) reported in the original article of Taskinen *et al.* 2014, where switchavidin

was studied comprehensively for the first time. The overall repeatability of the switchavidin layer was good as the corresponding coefficients of variation (CV; ratio of SD and arithmetic mean) were 3.7 % and 4.2 % for the upper and lower flow channel, respectively. The deviations in the immobilization level and repeatability of switchavidin binding may originate from the changes in the b-SAM deposition, which was not so optimized, but practically more straightforward. The challenges associated with the b-SAM quality are discussed later in the regeneration section. Further, the differing wavelengths of the instruments (785 nm for the MP-SPR and 760 nm for the Biacore setup) affect the sensitivity of the detection system, and correspondingly, the observed levels (in mDeg) of switchavidin binding.

The statistical analysis of the flow cell-specific switchavidin immobilization levels did not show a statistically significant relation between the flow channels so the quality of b-SAM surfaces seemed consistent within a single sensor. The statistical analysis done for the sensor-specific values instead revealed statistically significant difference between the sensors. This may result from numerous reasons related to the quality of the switchavidin immobilization solution or the b-SAM membrane. The poor batch-to-batch quality of the gold layer e.g. due to surface defects may expose the gold surface for the non-specific adsorption of switchavidin as the surface changes are neutralized that lead to more hydrophobic adsorption behavior. Furthermore, the defects on the gold layer as well as the variation in the oxidation state of the gold surface during the b-SAM deposition process may lead to an erratic and therefore unstable b-SAM that may lose biotinylated b-SAM components during the regeneration cycles (Srisombat *et al.* 2011).

The decreasing trend observed in the scatter plot of sensor-grouped switchavidin immobilization levels shown in Figure 9 indicates probably the incomplete regeneration of the sensing surface from adsorbed switchavidin molecules in the previous cycle, or the previously described effects of surface defects and oxidation states during the b-SAM surface production phase. This subsequently leads to a lower immobilization level in the next cycle until there is space available only for reversible interactions. A similar trend was seen in the Figure 12, which describes the relative regeneration efficiency of the switchavidin layer.

In summary, the switchavidin binding on the b-SAM was assessed as a repeatable and reproducible process. The surface quality of the b-SAM was consistent within the sensor slide, but minor statistical deviation was seen between the sensor slides. It should be noted that the possible sources of batch-to-batch variation, such as the oxidation state and surface quality of

the gold layer, may explain the statistical significance of the sensor-specific results, and they can be corrected easily by optimizing the manufacturing process (Mockus *et al.* 2014). A downward trend was observed for the switchavidin adsorption cycles, which may be explained by the variation in the gold and b-SAM surface qualities.

6.1.3 Mechanical adsorption model of switchavidin

The high affinity biotin-avidin-biotin bridges provide a robust way to immobilize ligands in biomedical, biosensing, and biotechnological applications. This, however, requires the stable divalent binding of avidin molecules on the biotinylated surface as the monovalent binding is a reversible process. The binding valency of avidin molecules has been studied recently by changing the surface coverage of biotin residues (Ray *et al.* 2015) as well as with purpose-designed synthetic streptavidin constructs that have lower number of biotin binding sites, but retained binding affinity (Dubacheva *et al.* 2017). These approaches utilized a quartz crystal microbalance with dissipation (QCM-D) and spectroscopic ellipsometry (SE) to produce reliable quantitative information about the binding valency of avidin molecules (Dubacheva *et al.* 2017).

This section tries to apply the described explanations into the MP-SPR measurement results obtained for the adsorption of switchavidin onto the biotinylated SAM surface. The aim is to expand the knowledge about the adsorption behavior of surface charge neutralized avidins and, in a broader context, to assess the suitability of the MP-SPR detection system for similar molecules that bind multivalently on the planar surface. From a commercial point of view, the reliable and real-time assessment tool for the binding valencies would benefit the development and quality assurance of multivalent ligands and corresponding surfaces. Further, it would improve the reproducibility and automation of different bioassays by providing complete monolayers of mediator or ligand molecules with less manual optimization.

In the first step, the switchavidin molecules bind randomly to biotin residues of b-SAM surface, and the protein covered area and the density of the adsorption layer increases. This process has been observed as a negative shift in the resonance frequency and as a positive shift in the dissipation energy and the ellipsometric surface coverage in the earlier studies for the streptavidin (Dubacheva *et al.* 2017) and the neutralized chimeric avidin (NCAvd) (Ray *et al.* 2015). The increase in the packing density of proteins i.e. the density of the adsorption layer, was probably detected during the switchavidin adsorption as an increase in the PMI signal as

this is sensitive to the optical scattering of the biomolecular layer (presented in Figure 10) (Viitala *et al.* 2013). The lateral interactions between the surface-bound neutralized switchavidin molecules may lead to a positive co-operation of switchavidin binding, and to a subsequent initiation of island formation (Rabe *et al.* 2011). Due to the immobile structure of b-SAM, this is, however, largely a local phenomenon in comparison with a mobile biotinylated supported lipid bilayer (b-SLB), in which biotinylated lipids can move by lateral diffusion (Reviakine and Brisson 2001).

Then, the switchavidin covered area and the fractional population of monovalently bound switchavidin molecules reach their maximum values. Simultaneously, the switchavidin molecules continue to minimize their energy state in a transitional phase, where the monovalently bound switchavidin molecules proceed towards multivalently bound switchavidin molecules. An overshoot peak and a subsequent decrease were observed in the dissipation shifts of the QCM-D systems during the association phase of switchavidin when the surface coverage of biotin residues in the b-SAM was higher than 0.5 % (Dubacheva *et al.* 2017 in Figure 5A; Ray *et al.* 2015 in Figure 6). These responses were also seen in the PMI signal of MP-SPR (presented in Figure 10). When the dissipation shift of QCM-D was plotted as a function of surface coverage measured with SE, the height of the overshoot peak lowered as the surface density of biotin residues increased (Ray *et al.* 2015 in Figure 8). This suggests that there is a structural difference between the adsorption layers formed on surfaces with high and low biotin content. Interestingly, a similar decline in the height of the overshoot peak was observed with the increasing number of regeneration cycles done for the switchavidin layer. The decrease after the overshoot peak indicates consistently a continuous mechanical stabilization of switchavidin molecules e.g. via protein – protein interactions as well as an entropy-driven hydrodynamic process, where the protein surface-bound water molecules dissociate during the adsorption onto the b-SAM surface (Bingen *et al.* 2008).

The critical packing density is achieved when a major part of the monovalently bound switchavidin molecules have been replaced by switchavidin molecules showing divalent binding. At this point, the protein – protein interactions increase significantly, which may trigger orientational changes in the switchavidin layer to optimize the electrostatic repulsions and attractions. Such reorganization may increase the total binding energy within the adsorbing protein molecules as well as of the solid surface – protein interactions (Rabe *et al.* 2011). This was potentially observed as a small although repeatable (N = 14) elevation in the PMI signal

(presented in Figure 10 with grey arrows). The shape of the dissipation shift during the adsorption of tetrameric streptavidin onto the b-SAM surface and, more clearly, onto the b-SLB, support this finding (Dubacheva *et al.* 2017 in Figures 5A and 5B). A similar trend was also seen during the adsorption of NCAvd onto the b-SAM surfaces with the surface coverage of biotin higher than 0.5 % (Ray *et al.* 2015). At the same time point when the critical packing density was achieved, the saturation limit of b-SAM was found for the switchavidin binding according to the new baseline of SPR peak minimum angle.

Granqvist and colleagues observed in 2013 a highly reminiscent overshoot effect in a similar but reversed system (labeled biotin binds surface immobilized avidin) measured with equivalent MP-SPR instrumentation. They suggested that the overshoot peak in the label-enhanced absorbance was caused by the sample plug of labeled biotin injection. Alternatively, a surface crystallization of avidins could explain the changes in the PMI as the optical scattering of the biomolecular layer increases as the size of protein clusters increases. This does not, however, provide explanation for the kinetic profile of switchavidin adsorption (Raynal *et al.* 2014).

The sensorgram of switchavidin adsorption onto the b-SAM surface included atypical adsorption profile (shown in Figure 19) that may originate from the low amounts of detergent residuals left into the immobilization solution of switchavidin (Biacore^{TM} Assay Handbook 2012). The purification of switchavidin had been performed with hand washed laboratory glassware, which may explain the residuals of detergents. The existence of detergents in the immobilization solution may affect the surface chemistry related to the adsorption mechanism. Therefore, the buffer exchange of the switchavidin solution would be an essential step in future studies if the mechanical adsorption model is studied more.

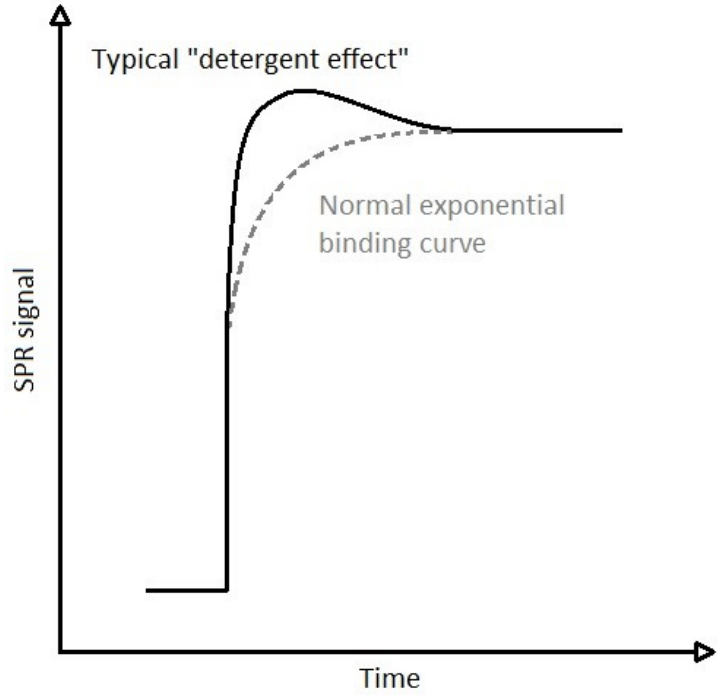

Figure 19. Schematic sensorgram showing typical detergent effect. The normal exponential binding curve is illustrated with grey dashed line. The figure was recreated based on Biacore™ Assay Handbook (2012).

To conclude, the MP-SPR detection system is not intended to provide a conclusive explanation to the multivalent adsorption behavior of switchavidin or avidin proteins, but rather to support the similar observations achieved with non-optical methods, such as QCM-D. The analysis of PMI signals deriving from the switchavidin adsorption event gave a strong direction for further studies related to the MP-SPR detection of multivalent binding. The binding valency of switchavidin could be studied more by alternating the surface coverage of biotin residues in the b-SAM as well as by using suitable reported molecules with proper controls as described in two reference articles earlier in this section (Ray *et al.* 2015; Dubacheva *et al.* 2017). The qualitative surface analysis of adsorbed proteins could be performed for example by atomic force microscopy (AFM) that would also provide adhesion and cohesion energy for the protein – protein and protein – surface interactions (Rabe *et al.* 2011), or by fluorescent microscope techniques, when biotinylated fluorescent tags e.g. biotin–4-fluorescein, are utilized (Taskinen *et al.* 2014).

6.1.4 Regeneration of immunosensing platform

According to the reference study presented by Zauner *et al.* in 2016, the normal regeneration of biotinylated protein G – anti-PSA interaction was relatively successful as only 2.4 % of switchavidin was found to be removed per cycle for the first two cycles. Further, this amount

decreased to 0.9 % for the subsequent cycles. The most probable reason for this decrease after the first two cycles is the desorption of unstable fractions of switchavidin by the normal regeneration solution. The obtained results were slightly better than the corresponding value calculated from the values reported in the reference studies, that is, 7.8 % (= 18.8 mDeg / 241.6 mDeg) (Zauner *et al.* 2016). The impact of non-specific switchavidin desorption was marginal as the reference flow channel (blocked with biotinylated BSA) acted in a similar way, and the referencing step was fully applicable.

The first rigorous regeneration of the switchavidin surface either left small residual amounts of proteins on the b-SAM, or alternatively resulted in a removal of all proteins from the b-SAM, or a tiny amount of biotinylated SAM components (as shown in Figure 11). After the first cycle, the amount of switchavidin residuals was on average +3.7 (SD 2.93) mDeg (CV 79 %) for the next few cycles that were performed. It is worth noticing that the reported sensor-specific baseline shift values for rigorous regeneration are unequal due to varying protein compositions on top of the switchavidin that may cross-link and prevent switchavidin molecules from desorbing locally.

The regeneration efficiency ratio in Figure 12 stabilized to 1.00 after sixth cycles, which means that all the adsorbed switchavidin molecules have been removed successfully from the b-SAM surface. From the perspective of assay development, it seems that the constant level of adsorbed switchavidin was found after the sixth cycle. This does not, however, reveal the adsorption mechanism (specific biotin-switchavidin interaction versus non-specific) of the switchavidin nor the amount of oriented i.e. available switchavidin.

In conclusion, the normal regeneration was efficient with a sufficient resolution to the rigorous regeneration. The first two normal regeneration cycles most likely removed a small fraction of weakly bound switchavidin. The use of accurate imaging techniques, such as AFM at different stages (e.g. the gold layer before and after b-SAM deposition as well as the b-SAM surface between the switchavidin immobilization and rigorous regeneration cycles), would shed some light on the real processes of sensing surface regeneration.

6.1.5 Anti-fouling ability of switchavidin layer

The switchavidin layer demonstrated clear ultra-low fouling ability against single protein solutions of BSA, lysozyme, and h-IgG based on the mean fouling SPR signal amplitudes (Brault *et al.* 2012). More closely, the mean fouling levels were lower than the specified

adsorption level of 5 mDeg, which corresponds roughly to 50 pg mm^{-2} or 2.4 % percent adsorption on the average switchavidin monolayer (~ 211 mDeg) (Vaisocherová *et al.* 2015). This result was in accordance with the results reported in the reference article of Zauner *et al.* (2016). Furthermore, the percent adsorption of lysozyme (0.2 %) was lower than that reported for the pure EG_3 SAM membrane (1 %), which indicates that the switchavidin monolayer improve the anti-fouling property of the system sensing surface (https://www.prochimia.com/products/product/1; July 22, 2017).

The completeness of the BSA blocking process remained unclear due to a large sensor-specific variation between the fouling levels of first and second BSA injection presented in Table 3. This variation could be explained with the surface defects on the gold layer and inconsistences on the SAM surface as noted in the immobilization and regeneration sections of switchavidin. Furthermore, the signal analysis of protein fouling was complicated due to low signal levels and strong downwards directed drifting. Incomplete i.e. a loosely packed BSA adsorption layer may lead to this drifting effect as a result of desorbing BSA molecules, and ultimately may compromise the stability of the sensing surface (Rabe *et al.* 2011).

In summary, the switchavidin layer that was bound on the b-SAM has ultra-low fouling properties against the single-protein solutions of BSA, h-IgG, and lysozyme. Overall, the total number of cycles was clearly insufficient to make statistical evaluations concerning the efficiency of BSA blocking or the anti-fouling ability against BSA, lysozyme, or h-IgG. The achieved results can be exploited only to guide further research. Next steps would be the confirmation of results with statistical significance. After that one can proceed to multicomponent protein solutions that mimic more closely the adsorption behavior of complex media, such as blood serum.

6.1.6 Kinetics of biotinylated protein G – anti-PSA interaction

The injections of anti-PSA dilutions were too short to analyze the kinetics and affinity of the anti-PSA – biotinylated protein G interactions reliably because the equilibrium phase of the interaction was not achieved. The results were obtained only from a single sensor so the statistical analysis of results was impossible and the quality of the Langmuir and bivalent fittings were poor. The reported kinetic values are, therefore, not very reliable. Chi^2-values are reasonable low, although, certain upper limit cannot be set for the Chi^2-value.

The chosen IgG (anti-PSA) from Medix Biochemica showed relatively strong affinity to the biotinylated protein G molecule based on the Langmuir model fitting shown in Figure 13. The dissociation constant was (0.766 ± 0.071) nM, which was consistent with the reference value of Zauner *et al.* (2.0 nM). The dissociation times were between 30 min to 1 hour depending on the concentration of the anti-PSA based dissociation curves in Figure 13.

The bivalent model gave a visually slightly better fit (shown in Figure 14) than the simple Langmuir model for the anti-PSA binding to biotinylated protein G molecules. This is most likely due to the "flexibility" of fitting algorithm used in the bivalent model. In fact, the closer inspection of kinetic parameters calculated for the bivalent phase of the binding showed that the standard deviations were relatively high and the bivalent model may not conform to what is happening on the sensing surface.

The residual plots for both kinetic fittings (Figure 15 and 16) showed a systematic deviation between the two highest and the rest of the anti-PSA concentrations, which may indicate the incapability of the available models to interpret the experimental situation (https://www.sprpages.nl/data-fitting/validation; July 22, 2017). The deviation was higher for the Langmuir model fitting than for the bivalent fitting, which may originate from the earlier mentioned flexibility of the fitting algorithm. The deviations in the interaction kinetics may originate from the aggregates or protein clusters of antibodies that interfere with the specific binding event on the biotinylated protein G layer (Rabe *et al.* 2011).

In conclusion, the bivalent model gave a better kinetic fit than the Langmuir model to some extent, but only for a single dilution series that inevitably cause uncertainty to the kinetic calculations. Overall, more measurement cycles are required with the higher concentration of antibodies under systematic quality control to assess the applicability of the immunosensing platform as well as to achieve more reliable kinetic results (Raynal *et al.* 2014).

6.2 Interaction kinetics of sulfonamide hCAII inhibitors

6.2.1 Immobilization of hCAII enzyme

The human carbonic anhydrase II enzyme (pI = 6.86; theoretical) was selected for the experiments instead of bovine carbonic anhydrase II (pI = 5.88; Rogez-Florent *et al.* 2014) as this resembles more closely the pharmacodynamics of human targeted CAII drugs.

The isoelectric points of these two allozymes were different so the pH of the hCAII immobilization solution was adjusted to pH 5.7 based on the standard operation procedure commonly used for the EDC/NHS amine coupling chemistry. The amine coupling chemistry interfering compounds, such as Tris-SO_4 and sodium azide, were removed from the hCAII stock solution by centrifugal ultrafiltration. The immobilization of hCAII at specific conditions resulted in an immobilization level of 675 mDeg, which was consistent with the immobilization level reported in the reference article of Papalia et al 2006 (690 mDeg on average). The dissociation constant of the hCAII – inhibitor interaction was assumed practically as independent on the level of enzyme immobilization based on the experimental data presented in the literature for the bovine CAII enzyme (Cannon *et al.* 2004). The pre-concentration testing conducted in further studies, however, revealed that the optimal pH for the hCAII immobilization solution could have been between pH 6.1 and 6.5 (data not shown). Unfortunately, the subsequent immobilization rounds failed in other ways e.g. due to air-bubble problems.

6.2.2 Detection of hCAII interaction kinetics with inhibitors

The main technical challenges in the pharmacodynamic studies of carbonic anhydrase inhibitors are related to the fast association kinetics of sulfonamide inhibitors (even in the order of 10^6 M^{-1} S^{-1} for AZE) combined with a small size of the inhibitor molecule (less than 400 Da) (Papalia *et al.* 2006). Furthermore, sulfonamide-based inhibitors are insoluble in water per se. Therefore, DMSO is used in the stock solution preparations as a standard operation procedure. The AZE inhibitor was, however, assessed as fully soluble in PBS with 3% of DMSO as the experiments conducted in the earlier study also without DMSO did not show a difference between the kinetic sensorgrams for the bovine CAII (Cannon *et al.* 2004).

Moderate quality kinetic data was obtained only from a single sensor with one dilution series for the AZE inhibitor due to the practical problems in the immobilization of hCAII as well as in the air bubble management. At first, the dissociation rate constant was fitted separately resulting in $(7.8 \pm 0.1) \times 10^{-3}$ s^{-1}. Then this was set as constant in the global Langmuir model fitting (presented in Figure 17). The additional mass transport term that was applied in the reference article of Papalia *et al.* in 2006 did not improve the Langmuir model fitting at any respect so it was not used in the kinetic analysis. The fitting algorithm did not find the association phase of the curves well, which caused some inaccuracy to the results. The B_{max} in turn was found accurately. The signal residuals obtained for the global Langmuir fitting of the

hCAII - acetazolamide interaction data (shown in Figure 18) were in the same level with the noise recorded for the enzyme-coupled sensing surface. This suggests that the instrumental noise does not limit the resolution of kinetics significantly in this system. The shape of the residuals, however, pointed out systematic deviations at the beginning of association and dissociation phases that suggests inadequate ability of the fitting algorithm to describe the interaction phenomenon fully.

The dissociation constant for the hCAII – AZE interaction was (16 ± 2) nM. This value was in accordance with the reference value of (20 ± 1) nM reported by Rogez-Florent *et al.* in 2013. The observed association [(0.49 ± 0.06) x 10^6 M^{-1} s^{-1}] and observed dissociation [(7.8 ± 0.1) x 10^{-3} $s^{-}1$] of AZE were slower than the reference values: k_a = (1.7 ± 0.7) x 10^6 M^{-1} s^{-1} and k_d = (7.8 ± 0.1) x 10^{-3} s^{-1}. This may result from diffusion-limited kinetics and re-binding of AZE molecules with hCAII enzymes in the thick CMD matrix, which ultimately affects both the association and dissociation rate constants in a similar extent and leave dissociation constant ($K_D = k_d / k_a$) unaltered (Papalia *et al.* 2006). In the protocol of Rogez-Florent *et al.* (2013), the effect of MTL was minimized by using a flow rate of 100 µl min^{-1}, which suggests that the difference originates possibly from the MTL present in the experiment setup.

The rapid association phase of the AZE binding requires a very good time resolution of the SPR instrument. The MP-SPR Navi™ instrumentation utilizes the angular scan to record the full SPR curve and to monitor RI changes in the bulk phase, which in turn lowers the time resolution and complicates the detection of fast association kinetics. In the case of AZE, it was, however, possible to measure association kinetics in the scale of 10^5 M^{-1} s^{-1}. Sometimes, the disadvantage related to the angular scan can be compensated with a PureKinetics™ tool (BioNavis) that subtracts the TIR change directly from the SPR peak minimum angle, and helps to distinguish the association curvature from the bulk change. The low signal levels of small molecules, however, emphasize the combined noise level deriving from both the TIR angle signal as well as the peak minimum angle signal resulting in low signal-to-noise ratio. Therefore, PureKinetics™ tool was not applicable in this context. The fixed angle mode that can be applied also in the MP-SPR Navi™ instrumentation improves the time resolution of measurement significantly.

The serial injection of the running buffer (3 % DMSO in PBS) from the 96-well plate showed unusually high bulk effect in both the active and reference channel of the sensorgram (not

shown) despite the intensive washing procedures performed for the fluidic system. This indicates the excluded volume effect that was corrected in the reference article of Papalia *et al.* 2006 with a calibration series of DMSO. Alternatively, the use of deactivated recombinant (mutated) or denatured form of hCAII in one of the reference channels could alleviate the problem.

In the original protocol of Papalia *et al.* 2006, the re-sealable soft rubber caps with glass vials were used. In this experimental work, the plastic 96-well-plates were used without any film to cover the wells filled with analyte dilutions. Furthermore, it was noted later that the buffer containers turned their color from white to yellowish after a few days' storage of running buffer containing 3% DMSO. Despite the effort to prepare samples and buffers right before use, the evaporation and absorption to plastics may have affected the results. This should be taken into consideration in further studies.

In conclusion, the detection of rapid small molecule interaction kinetics was clearly dependent on the performance of a 4-channel MP-SPR prototype in terms of instrumental noise and time resolution, but the successful immobilization of hCAII into CMD matrix, the stabilization of the sensing surface and the careful preparation of buffers and analyte dilutions play a key role for the visible binding kinetics as well. In future studies, it should be noted that correction of the excluded volume effect as well as the optimization of sample preparation regarding the right use of DMSO may improve the quality of kinetic data. The effect of MTL could be reduced by increasing the flow rate, e.g. to 100 µl min^{-1}. The fixed angle mode would also provide a higher sampling frequency.

7 CONCLUSIONS

The regenerable and stable immunosensing platform based on the switchavidin and protein G molecules was reconstructed. This system showed high repeatability and reproducibility in terms of baseline drift of b-SAMs, switchavidin immobilization, regenerability, and anti-fouling ability. The affinity immobilization of antibodies to the biotinylated protein G monolayer requires more research with higher concentrations of high-quality antibodies to achieve the saturation limit that enables the higher sensitivity of the immunoassay system. The stability of mediator molecules as well as the binding valency between the biotinylated protein G and IgG molecules will determine the expected detection limit and the stability of the immunosensing platform. The antifouling ability of the immunosensing platform could be tested with multicomponent protein solutions in the next phase to evaluate the resistance against the cooperative non-specific binding of proteins.

The systematically repeating overshoot peak, logarithmic decrease, and small elevation in the PMI signal during the switchavidin adsorption was supported by similar observations found from the literature (Ray *et al.* 2015; Dubacheva *et al.* 2017). The mechanical adsorption model based purely on previous findings suggests that the MP-SPR might enable the monitoring of the multivalent binding process of switchavidin (overshoot peak and logarithmic decrease) as well as the optimization of protein – protein and protein – surface interactions (elevation). The development and quality assurance of multivalent ligands and corresponding surfaces would benefit from the real-time evaluation of multivalent binding processes. Further, the real-time monitoring of multivalent binding would improve the reproducibility and automation of different bioassays by providing complete monolayers of mediator or ligand molecules with less manual optimization. The proposed adsorption model, however, requires complimentary data measured for instance by AFM or fluorescent microscope techniques to validate the observations.

The kinetics of the hCAII enzyme – sulfonamide inhibitor interaction was resolved for AZE by immobilizing the hCAII enzyme into a CMD matrix and introducing the dilutions series of AZE with specified association and dissociation time. Notably, the physico-chemical conditions, where the carbonic anhydrase immobilization was performed, were different between the alloenzymes of human and bovine, most likely due to clearly differing isoelectric points (6.86 and 5.88, respectively). The kinetic data was measured using MP-SPR instrument of

BioNavis company in the angular scan mode. The time resolution of the angular scan seemed sufficient to record the rapid association kinetics of sulfonamide inhibitors in the scale of 10^5 M^{-1} s^{-1} for AZE. The unique PureKinetics™ tool was able to filter out some of the bulk signal. However, the small MW of sulfonamide inhibitors in addition to the plausible excluded volume effect of DSMO resulted in a low signal-to-noise ratio, and the overall quality of kinetic data was poor. The kinetic analysis, with kinetic values in the same range as those reported in literature, demonstrated that the detection of fast association kinetics of small MW analytes is possible using the MP-SPR instrumentation. The comparison of kinetic values with the reference values presented in the literature also highlighted that the kinetic data may contain a MTL factor, which can be corrected easily by increasing the flow rate of the system. In future studies, it is important that the calibration curve of DMSO is applied or a non-active enzyme is immobilized in one of the reference channels to remove the excluded volume effect. Finally, the kinetic measurements should be performed at least in triplicate to achieve statistically significant results.

8 REFERENCES

Armbruster, D.A. and Pry, T. 2008. Limit of blank, limit of detection and limit of quantitation. Clin. Biochem. Rev. 29 Suppl 1; S49-52.

Barnes, G. and I. Gentle. *Interfacial science: an introduction* [Book]. 2011. pp. 352. Oxford University Press, Oxford, UK.

Biacore™ Assay Handbook [Book]. 2012, pp. 78. GE Healthcare Bio-Sciences AB, Uppsala, Sweden.

Bingen, P., Wang, G., Steinmetz, N.F., Rodahl, M., and Richter, R.P. 2008. Solvation effects in the quartz crystal microbalance with dissipation monitoring response to biomolecular adsorption. A phenomenological approach. Anal. Chem. 80(23); 8880-8890.

Brault, N.D., Sundaram, H.S., Li, Y., Huang, C., Yu, Q., and Jiang, S. 2012. Dry film refractive index as an important parameter for ultra-low fouling surface coatings. Biomacromolecules. 13(3); 589-593.

Brena, B., González-Pombo, P., and Batista-Viera, F. *Immobilization of enzymes: a literature survey;* 15-30. *Immobilization of Enzymes and Cells* [Book]. 2013. Third edition. Humana Press, Springer. New York, NY.

Cannon, M.J., Papalia, G.A., Navratilova, I. *et al.* 2004. Comparative analyses of a small molecule/enzyme interaction by multiple users of Biacore technology. Anal. Biochem. 330(1); 98-113.

Clark, L. 1956. Monitor and control of blood and tissue oxygen tensions. Transactions of the American Society for Artificial Internal Organs. 2(1); 41-48.

Cooper, M.A. 2002. Optical biosensors in drug discovery. Nature reviews. Drug discovery. 1(7); 515-528.

Couture, M., Zhao, S.S., and Masson, J. 2013. Modern surface plasmon resonance for bioanalytics and biophysics. Physical Chemistry Chemical Physics. 15(27); 11190-11216.

Davidoff, S.N., Ditto, N.T., Brooks, A.E., Eckman, J., and Brooks, B.D. *Surface plasmon resonance for therapeutic antibody characterization;* 35-76. *Label-Free Biosensor Methods in Drug Discovery* [Book]. 2015. Humana Press, Springer. New York, NY.

Dubacheva, G.V., Araya-Callis, C., Geert Volbeda, A. *et al.* 2017. Controlling Multivalent Binding through Surface Chemistry: Model Study on Streptavidin. J. Am. Chem. Soc. 139(11); 4157-4167.

Fischer, M.J. *Amine coupling through EDC/NHS: a practical approach;* 55-73. *Surface plasmon resonance: methods and protocols* [Book]. 2010. Humana Press, Springer. New York, NY.

Frostell-Karlsson, Å., Remaeus, A., Roos, H. *et al.* 2000. Biosensor analysis of the interaction between immobilized human serum albumin and drug compounds for prediction of human serum albumin binding levels. J. Med. Chem. 43(10); 1986-1992.

Gasteiger, E.*, et al. Protein identification and analysis tools on the ExPASy server*; 571-607. *The Proteomics Protocols Handbook* [Book]. 2005. Humana Press, Springer. New York, NY.

Guo, X. 2012. Surface plasmon resonance based biosensor technique: a review. Journal of biophotonics. 5(7); 483-501.

Helmerhorst, E., Chandler, D.J., Nussio, M., and Mamotte, C.D. 2012. Real-time and Label-free Bio-sensing of Molecular Interactions by Surface Plasmon Resonance: A Laboratory Medicine Perspective. Clin. Biochem. Rev. 33(4); 161-173.

Homola, J. 2008. Surface plasmon resonance sensors for detection of chemical and biological species. Chem. Rev. 108(2); 462-493.

Huang, Y., Ho, H.P., Kong, S.K., and Kabashin, A.V. 2012. Phase-sensitive surface plasmon resonance biosensors: methodology, instrumentation and applications. Annalen der Physik. 524(11); 637-662.

International Union of Pure and Applied Chemistry (IUPAC). *Compendium of Chemical Terminology: Gold Book* [Book]. 2014. pp. 1622.

Johansen, K., Stålberg, R., Lundström, I., and Liedberg, B. 2000. Surface plasmon resonance: instrumental resolution using photo diode arrays. Measurement Science and Technology. 11(11); 1630.

Kurihara, K. and Suzuki, K. 2002. Theoretical understanding of an absorption-based surface plasmon resonance sensor based on Kretchmann's theory. Anal. Chem. 74(3); 696-701.

Laitinen, O., Hytönen, V., Nordlund, H., and Kulomaa, M. 2006. Genetically engineered avidins and streptavidins. Cellular and Molecular Life Sciences CMLS. 63(24); 2992-3017.

Li, Y., Liu, X., and Lin, Z. 2012. Recent developments and applications of surface plasmon resonance biosensors for the detection of mycotoxins in foodstuffs. Food Chem. 132(3); 1549-1554.

Mariani, S. and Minunni, M. 2014. Surface plasmon resonance applications in clinical analysis. Analytical and bioanalytical chemistry. 406(9-10); 2303-2323.

Mockus, L., Peterson, J.J., Lainez, J.M., and Reklaitis, G.V. 2014. Batch-to-batch variation: a key component for modeling chemical manufacturing processes. Organic Process Research & Development. 19(8); 908-914.

Nabok, A. and Tsargorodskaya, A. 2008. The method of total internal reflection ellipsometry for thin film characterisation and sensing. Thin Solid Films. 516(24); 8993-9001.

Nallani, M., Andreasson-Ochsner, M., Tan, C.D. *et al.* 2011. Proteopolymersomes: In vitro production of a membrane protein in polymersome membranes. Biointerphases. 6(4); 153-157.

Olaru, A., Bala, C., Jaffrezic-Renault, N., and Aboul-Enein, H.Y. 2015. Surface plasmon resonance (SPR) biosensors in pharmaceutical analysis. Crit. Rev. Anal. Chem. 45(2); 97-105.

Papalia, G.A., Leavitt, S., Bynum, M.A. *et al.* 2006. Comparative analysis of 10 small molecules binding to carbonic anhydrase II by different investigators using Biacore technology. Anal. Biochem. 359(1); 94-105.

Pollheimer, P., Taskinen, B., Scherfler, A. *et al.* 2013. Reversible biofunctionalization of surfaces with a switchable mutant of avidin. Bioconjugate Chem. 24(10); 1656-1668.

Pop-Georgievski, O., Rodriguez-Emmenegger, C., de los Santos Pereira, Andres, Proks, V., Brynda, E., and Rypáček, F. 2013. Biomimetic non-fouling surfaces: extending the concepts. Journal of Materials Chemistry B. 1(22); 2859-2867.

Rabe, M., Verdes, D., and Seeger, S. 2011. Understanding protein adsorption phenomena at solid surfaces. Adv. Colloid Interface Sci. 162(1); 87-106.

Ray, S., Steven, R.T., Green, F.M. *et al.* 2015. Neutralized Chimeric Avidin Binding at a Reference Biosensor Surface. Langmuir. 31(6); 1921-1930.

Raynal, B., Lenormand, P., Baron, B., Hoos, S., and England, P. 2014. Quality assessment and optimization of purified protein samples: why and how?. Microbial cell factories. 13(1); 180.

Reviakine, I. and Brisson, A. 2001. Streptavidin 2D crystals on supported phospholipid bilayers: toward constructing anchored phospholipid bilayers. Langmuir. 17(26); 8293-8299.

Rogez-Florent, T., Duhamel, L., Goossens, L. *et al.* 2014. Label-free characterization of carbonic anhydrase—novel inhibitor interactions using surface plasmon resonance, isothermal titration calorimetry and fluorescence-based thermal shift assays. Journal of Molecular Recognition. 27(1); 46-56.

Rutgers, A., Meyers, K.E., Canziani, G., Kalluri, R., Lin, J., and Madaio, M.P. 2000. High affinity of anti-GBM antibodies from Goodpasture and transplanted Alport patients to α3 (IV) NC1 collagen. Kidney Int. 58(1); 115-122.

Schasfoort, R.B. *Handbook of surface plasmon resonance* [Book]. 2017. pp. 403. Royal Society of Chemistry.

Sexton, B., Feltis, B., and Davis, T. 2008. Characterisation of gold surface plasmon resonance sensor substrates. Sensors and Actuators A: Physical. 141(2); 471-475.

Sippel, K.H., Robbins, A.H., Domsic, J., Genis, C., Agbandje-McKenna, M., and McKenna, R. 2009. High-resolution structure of human carbonic anhydrase II complexed with acetazolamide reveals insights into inhibitor drug design. Acta Crystallographica Section F: Structural Biology and Crystallization Communications. 65(10); 992-995.

Srisombat, L., Jamison, A.C., and Lee, T.R. 2011. Stability: A key issue for self-assembled monolayers on gold as thin-film coatings and nanoparticle protectants. Colloids Surf. Physicochem. Eng. Aspects. 390(1); 1-19.

Taskinen, B., Zauner, D., Lehtonen, S.I. *et al.* 2014. Switchavidin: Reversible biotin–avidin–biotin bridges with high affinity and specificity. Bioconjug. Chem. 25(12); 2233-2243.

Thévenot, D.R., Toth, K., Durst, R.A., and Wilson, G.S. 2001. Electrochemical biosensors: recommended definitions and classification. Biosensors and Bioelectronics. 16(1); 121-131.

Trilling, A.K., Harmsen, M.M., Ruigrok, V.J., Zuilhof, H., and Beekwilder, J. 2013. The effect of uniform capture molecule orientation on biosensor sensitivity: dependence on analyte properties. Biosensors and Bioelectronics. 40(1); 219-226.

Vaisocherová, H., Brynda, E., and Homola, J. 2015. Functionalizable low-fouling coatings for label-free biosensing in complex biological media: advances and applications. Analytical and bioanalytical chemistry. 407(14); 3927-3953.

Vallée, P., Lafait, J., Legrand, L., Mentré, P., Monod, M., and Thomas, Y. 2005. Effects of pulsed low-frequency electromagnetic fields on water characterized by light scattering techniques: role of bubbles. Langmuir. 21(6); 2293-2299.

Viitala, T., Granqvist, N., Hallila, S., Raviña, M., and Yliperttula, M. 2013b. Elucidating the signal responses of multi-parametric surface plasmon resonance living cell sensing: a comparison between optical modeling and drug–mdckii cell interaction measurements. PloS one. 8(8); e72192. https://doi.org/10.1371/journal.pone.0072192

Weng, X., Gaur, G., and Neethirajan, S. 2016. Rapid detection of food allergens by microfluidics ELISA-based optical sensor. Biosensors. 6(2); 24.

Zauner, D., Taskinen, B., Eichinger, D. *et al.* 2016. Regenerative biosensor chips based on switchable mutants of avidin—A systematic study. Sensors Actuators B: Chem. 229; 646-654.

Zhang, H., Boussaad, S., and Tao, N. 2003. High-performance differential surface plasmon resonance sensor using quadrant cell photodetector. Rev. Sci. Instrum. 74(1); 150-153.